

Matrix-less methods for the spectral approximation of large non-Hermitian Toeplitz matrices: A concise theoretical analysis and a numerical study

Manuel Bogoya¹ | Sven-Erik Ekström² | Stefano Serra-Capizzano^{2,3} | Paris Vassalos⁴

¹Departamento de Matemáticas,
Universidad del Valle, Cali, Colombia

²Division of Scientific Computing,
Department of Information Technology,
Uppsala University, Uppsala, Sweden

³Dipartimento di Scienza e Alta
Tecnologia, University of Insubria,
Como, Italy

⁴School of Information Sciences, Athens
University of Economics and Business,
Athens, Greece

Correspondence

Sven-Erik Ekström, Division of Scientific Computing, Department of Information Technology, Uppsala University, Box 337, SE-751 05 Uppsala, Sweden.

Email: sven-erik.ekstrom@it.uu.se

Funding information

Athens University of Economics and Business; European High-Performance Computing Joint Undertaking; European Union's Horizon 2020 research and innovation programme

Abstract

It is known that the generating function of a sequence of Toeplitz matrices may not describe the asymptotic distribution of the eigenvalues of the considered matrix sequence in the non-Hermitian setting. In a recent work, under the assumption that the eigenvalues are real, admitting an asymptotic expansion whose first term is the distribution function, fast algorithms computing all the spectra were proposed in different settings. In the current work, we extend this idea to non-Hermitian Toeplitz matrices with complex eigenvalues, in the case where the range of the generating function does not disconnect the complex field or the limiting set of the spectra, as the matrix-size tends to infinity, has one nonclosed analytic arc. For a generating function having a power singularity, we prove the existence of an asymptotic expansion, that can be used as a theoretical base for the respective numerical algorithm. Different generating functions are explored, highlighting different numerical and theoretical aspects; for example, non-Hermitian and complex symmetric matrix sequences, the reconstruction of the generating function, a consistent eigenvalue ordering, the requirements of high-precision data types. Several numerical experiments are reported and critically discussed, and avenues of possible future research are presented.

KEY WORDS

asymptotic expansion, eigenvalues, GLT sequences, numerical algorithm, spectral symbols, Toeplitz matrices

1 | INTRODUCTION

Given a function $f \in L^p([-\pi, \pi])$ with $p \geq 1$, their Fourier coefficients \hat{f}_k are defined as

$$\hat{f}_k \equiv \frac{1}{2\pi} \int_{-\pi}^{\pi} f(\theta) e^{-ik\theta} d\theta, \quad i^2 = -1, \quad k \in \mathbb{Z}.$$

This is an open access article under the terms of the [Creative Commons Attribution License](#), which permits use, distribution and reproduction in any medium, provided the original work is properly cited.

© 2024 The Authors. *Numerical Linear Algebra with Applications* published by John Wiley & Sons Ltd.

In the particular case $f \in L^2([-\pi, \pi])$ it is well-known that $f(\theta)$ coincides with its Fourier series $\sum_{k=-\infty}^{\infty} \hat{f}_k e^{ki\theta}$, but for any $p \geq 1$ the $n \times n$ Toeplitz matrix $T_n(f)$ is given by

$$T_n(f) = \left[\hat{f}_{i-j} \right]_{i,j=1}^n = \begin{bmatrix} \hat{f}_0 & \hat{f}_{-1} & \cdots & \hat{f}_{2-n} & \hat{f}_{1-n} \\ \hat{f}_1 & \ddots & \ddots & & \hat{f}_{2-n} \\ \vdots & \ddots & \ddots & \ddots & \vdots \\ \hat{f}_{n-2} & & \ddots & \ddots & \hat{f}_{-1} \\ \hat{f}_{n-1} & \hat{f}_{n-2} & \cdots & \hat{f}_1 & \hat{f}_0 \end{bmatrix}.$$

In this setting the function f is called the *generating function* of $T_n(f)$. There are two standard ways of working with generating functions, the first one (mostly used by the numerical community) is to consider a function over a real interval of the kind $[0, 2\pi]$ or $[-\pi, \pi]$, and the second one (mostly used by the operator theory community) is to consider a function over the complex unit circumference $\mathbb{T} = \partial\mathbb{D}$ where \mathbb{D} is the complex unit disk. Noticing that a real variable θ in one of those intervals can be transformed into the complex variable $t = e^{i\theta}$, the two alternatives become equivalent.

Since the beginning of the 20th century, Toeplitz matrices had enjoyed plenty of applicability including engineering, stochastic processes, time series analysis, signal processing, image processing, quantum, and statistical mechanics. Moreover, the discretization of a differential operator on a uniform spatial grid, using Finite Differences (FD), Finite Elements (FE), Discontinuous Galerkin (DG), or even Isogeometrical Analysis (IgA), leads to a generally large linear system governed by a Toeplitz or Toeplitz-like matrix.

If one has, for example, the task of calculating the eigenvectors of $T_n(f)$ for designing an iterative algorithm to solve the linear system $T_n(f)x = b$, the distribution of the set $\text{spt}_n(a)$ is of little or no help, because in such a case the individual eigenvalues are necessary. Then, the easiest option seems to be the usage of any standard eigensolver (such as `Eigenvalues` in MATHEMATICA, `eig` in MATLAB, or `eigvals` in JULIA) but they can fail and produce fundamentally incorrect results. In general terms, those difficulties are related to the condition number (e.g., of the eigenvector matrix), limited precision, the proximity between eigenvalues, and the sparse nature of the matrix.

For instance, the condition number of a Hermitian positive definite matrix arising from the discretization of a coercive self-adjoint partial differential operator is known to be proportional to the ratio between the largest eigenvalue and the smallest eigenvalue, hence they are ill-conditioned polynomially in the matrix size, with exponent depending on the highest involved derivatives. The size of this kind of matrices is the number of considered grid points, typically in the range of 10^5 – 10^8 , therefore the numerical calculation of its eigenvalues leads to large memory consumption. In addition, standard eigensolvers are non-parallel and have time complexities approaching the order $O(n^3)$ where n is the matrix size. As a consequence, it is desirable to have a more efficient alternative, such as an individual eigenvalue expansion.

A further notion which is of crucial relevance to our study is that of spectral symbol which we report below for general matrix sequences. In fact, it is important to keep the concepts of generating function and spectral symbol distinct, the one of generating function f for a Toeplitz matrix sequence $\{T_n(f)\}_n$ and that of spectral symbol \mathfrak{f} for a general matrix sequence, because they are often confused (for these concepts, related notions, and applications see the books^{1–4}) and the exposition for Engineers.⁵

Definition 1. Let $\mathfrak{f} : [a, b] \rightarrow \mathbb{C}$ be a measurable function in the Lebesgue sense. Assume that $\{A_n\}_n$ is a sequence of matrices with eigenvalues $\lambda_j(A_n)$ ($j = 1, \dots, d_n$) and such that $\dim(A_n) = d_n \rightarrow \infty$ as $n \rightarrow \infty$. We say that $\{A_n\}_n$ is *distributed as \mathfrak{f} over $[a, b]$ in the sense of the eigenvalues*, or that \mathfrak{f} is the *spectral symbol* of $\{A_n\}_n$, and we write $\{A_n\}_n \sim_{\lambda} (\mathfrak{f}, [a, b])$ if

$$\lim_{n \rightarrow \infty} \frac{1}{d_n} \sum_{j=1}^{d_n} F(\lambda_j(A_n)) = \frac{1}{b-a} \int_a^b F(\mathfrak{f}(t)) dt, \quad (1)$$

for every continuous function F with compact support.

The eigenvalue ordering plays an important role in the individual expansions treated in this work, but in the previous definition it is not necessary and therefore, it is not assumed. Throughout the paper, when the domain can be easily inferred from the context, we will replace the notation $\{A_n\}_n \sim_{\lambda} (\mathfrak{f}, [a, b])$ with $\{A_n\}_n \sim_{\lambda} \mathfrak{f}$.

Remark 1. When f is smooth enough, an informal interpretation of the limit relation (1) is the following: if n is sufficiently large, then up to a negligible—at most $o(d_n)$ —possible outliers, the eigenvalues of A_n can be approximated by a sampling of f on a uniform grid of the domain $[a, b]$. We notice that here the adjective “negligible” has a specific meaning in a theoretical sense, since the related number of outliers divided by d_n tends to zero as n tends to infinity. From a practical viewpoint, for example, in the estimate of convergence of (preconditioned) Krylov methods, we are interested in a more precise quantification with the number of outliers growing mildly with n and possibly bounded by a constant independent of n .

In the Toeplitz setting, when the notions of f and \mathfrak{f} coincide, that is when $\{T_n(f)\}_n \sim_\lambda (f, [-\pi, \pi])$, it is customary to say that the eigenvalues of $T_n(f)$ have *canonical distribution*. The Szegő classical results⁶ show that this is the case for a real-valued function in $L^\infty([-\pi, \pi])$. Under this approach, in 1990 Widom⁷ was able to prove that the canonical distribution also holds if f is a continuous complex-valued function having a power singularity over \mathbb{T} , and he raised the following clever conjecture:

Exceptions from canonical distribution of the eigenvalues of $T_n(f)$ can only occur when f extends analytically to an annulus $r < |z| < 1$ or $1 < |z| < R$,

which has been verified in a number of particular cases but remains unsolved.

Let \mathcal{TC} be the collection of all $f \in L^\infty([-\pi, \pi])$ such that its essential range $\mathcal{ER}(f)$ does not disconnect the complex plane and has empty interior. Later on, in 1998 Tilli^{8,9} proved that if f belongs to \mathcal{TC} , then we will have canonical distribution as well, and this is why we called \mathcal{TC} the *Tilli class*.

Theorem 1. Let $f \in \mathcal{TC}$, then $\{T_n(f)\}_n \sim_\lambda (f, [-\pi, \pi])$ that is $f = \mathfrak{f}$. If the function ωf is real-valued almost everywhere (a.e.) for some complex unitary constant ω , then f belongs automatically to the Tilli class \mathcal{TC} , and therefore $f = \mathfrak{f}$. This is also true in the more general case of a real-valued $\omega f \in L^1([-\pi, \pi])$. Furthermore, when f is non constant and real-valued a.e., all the eigenvalues of $T_n(f)$ belong to the open interval (m, M) , where m and M are the essential infimum and the essential supremum of f , respectively. In the case where f is constant a.e., that is $f = m = M$ a.e., the result is trivial since $T_n(f) \equiv mI_n$ with I_n being the identity matrix of order n .

Theorem 1 turns out to be a compilation of the research carried out in the last 100 years, the distribution results can be found in References 8 and 9 and the localization results are in References 10 and 11. Moreover, in the Toeplitz setting and in connection with Remark 1, the assumption that f is real-valued a.e. implies that there are no outliers. See the books^{1–4} and the references therein.

Considering f as a function of $t \in \mathbb{T}$, in 1960 Schmidt and Spitzer¹² introduced the limiting set $\Lambda(f)$ of the spectra $\text{sp}T_n(f)$, as

$$\Lambda(f) \equiv \limsup_{n \rightarrow \infty} \text{sp } T_n(f), \quad (2)$$

consisting in all the complex points λ for which there exists a sequence $n_1 < n_2 < \dots$ and $\lambda_{n_k} \in_{n_k}^T (f)$ such that $\lambda_{n_k} \rightarrow \lambda$ as $k \rightarrow \infty$. As a consequence, as $n \rightarrow \infty$ the set $\text{sp}T_n(f)$ converges to $\Lambda(f)$ in the Hausdorff metric. When f is a Laurent polynomial (equivalently $T_n(f)$ is banded) they proved that $\Lambda(f)$ is related to the range $\mathcal{R}(f)$ in a nontrivial way, forming a connected set encircled by $\mathcal{R}(f)$ which is the union of finite analytic arcs together with their end points. Moreover, in 1967 Hirschman¹³ proved that the spectra $\text{sp}T_n(f)$ are distributed over $\Lambda(f)$, and in 1975 Day¹⁴ extended the results of Schmidt–Spitzer and Hirschman to an arbitrary rational function without poles on \mathbb{T} .

Hence, if f (considered as a function of $t \in \mathbb{T}$) is a Laurent polynomial or a rational function without poles on \mathbb{T} then, in general, the eigenvalues of $T_n(f)$ are not canonically distributed (equivalently $\{T_n(f)\}_n \not\sim_\lambda f$). The determination of canonical distribution can be done with an individual eigenvalue expansion, but in general it has proved to be difficult and is still an open problem. There is no literature (theoretical or numerical) regarding the individual eigenvalue expansion in the noncanonical case, even though, in the present work we study cases with and without canonical distribution.

The precise calculation of $\Lambda(f)$ is, in general, a challenging task. Recently, Böttcher et al.¹⁵ proposed a novel numerical algorithm to approximate $\Lambda(f)$ with high accuracy and moderate computational cost. Nevertheless, in this article, we will rely on the algorithm proposed by Ekström and Vassalos,¹⁶ because it produces an expression for \mathfrak{f} instead of its range.

With this connection we introduce the class \mathcal{T} as the collection of all generating functions $f \in L^1(-\pi, \pi)$ satisfying one of the following conditions,

- (i) f belongs to the Tilli class \mathcal{TC} and the essential range $\mathcal{ER}(f)$ is connected,
- (ii) the limiting set $\Lambda(f)$ has one nonclosed analytic arc only.

According to Theorem 1, in case (i) we have canonical distribution and $\Lambda(f) = \mathcal{ER}(f) = \mathcal{ER}(\mathfrak{f})$. In case (ii), f does not necessarily coincide with \mathfrak{f} but since the eigenvalues of $T_n(f)$ approach $\Lambda(f)$ in the Hausdorff metric and $\{T_n(f)\}_n \sim_{\lambda} \mathfrak{f}$, we obtain $\Lambda(f) = \mathcal{ER}(\mathfrak{f})$. Therefore, in both cases $\mathcal{ER}(\mathfrak{f})$ is a nonclosed connected curve having only two endpoints, and then we propose a general ordering strategy, *to enumerate the eigenvalues from one end to the other*.

In a recent work¹⁶ the cases of interest were those in which $\{T_n(f)\}_n \sim_{\lambda} f$ and the eigenvalues of $T_n(f)$ are real for all n . In such a setting, often the matrix sequence $\{T_n(f)\}_n$ is such that there exists a real-valued function \mathfrak{f} satisfying $\{T_n(f)\}_n \sim_{\lambda} \mathfrak{f}$, with the eigenvalues of $T_n(f)$ admitting an asymptotic expansion of the same type as considered in previous theoretical^{17,18} and numerical^{19–21} works. We call methods that numerically approximate this asymptotic expansion *matrix-less* if, after the respective precomputing phase, the eigenvalue computation does not need to work in any way with the related matrix. Recent literature had studied the real-valued,^{16,19} preconditioned,²⁰ banded block,²¹ parallel,²² and B-spline IgA²³ settings. Böttcher et al.,¹⁵ besides the rich and crystal clear theoretical study, presented an algorithm in the spirit of that of Beam and Warming.²⁴

We remark that when $f \neq \mathfrak{f}$, that is, when the eigenvalues of $T_n(f)$ are not canonically distributed, there is no theoretical nor numerical results involving an individual asymptotic expansion. In this paper we extend this notion to the case where the eigenvalues of $T_n(f)$ are complex-valued for each n . We write $f(\theta) = f^{\Re}(\theta) + i f^{\Im}(\theta)$ and assume that there exists a function $\mathfrak{f}(\theta) = \mathfrak{f}^{\Re}(\theta) + i \mathfrak{f}^{\Im}(\theta)$ that describes the eigenvalue distribution of $T_n(f)$.

The paper is organized as follows. In Section 2 we prove the existence of an asymptotic eigenvalue expansion which we use to formulate a general Working Hypothesis (WH). In Section 3 we present representative examples for testing WH. In Section 4 we describe in Algorithm 1 the numerical approach for approximating the coefficients in the expansion. In Section 5 we present numerical results for the previously defined examples. Finally, in Section 6 we present our conclusions, discuss the presented results, and possible future research avenues.

2 | MAIN RESULTS

In this section, in a particular case, we prove the existence of an asymptotic eigenvalue expansion, which is used later on to formulate a general WH.

In the late sixties, Fisher and Hartwig²⁵ studied a collection of generating functions which, according to them, were the most needed by the scientific community. They described them as having the structure

$$a(t) = b(t) \prod_{k=1}^m \left(1 - \frac{t_k}{t}\right)^{\mu_k} \left(1 - \frac{t}{t_k}\right)^{\nu_k},$$

where b is a nonvanishing and sufficiently smooth function over \mathbb{T} , having winding number zero about the origin, t_1, \dots, t_m , are pairwise distinct points on \mathbb{T} , and μ_k, ν_k ($k = 1, \dots, m$) are complex numbers selected in such a way that a belongs to $L^1(\mathbb{T})$. Since then, this collection is known as the *Fisher–Hartwig class* and has attracted a large amount of related studies. The book²⁶ is a nice reference for the many associated details. As a consequence, we opted to work with a generating function in the Fisher–Hartwig class.

Let H^∞ be the Hardy space of (boundary values of) bounded analytic functions in \mathbb{D} . For a continuous generating function $a : \mathbb{T} \rightarrow \mathbb{C}$, we denote by

$$\text{wind}_\lambda(a) \equiv \frac{1}{2\pi i} \oint_{\mathcal{R}(a)} \frac{d\zeta}{\zeta - \lambda},$$

the winding number of a in connection with a point $\lambda \in \mathbb{C} \setminus \mathcal{R}(a)$. Intuitively, $\text{wind}_\lambda(a)$ is the number of times that the range $\mathcal{R}(a)$ travels around the point λ in counterclockwise sense. We also denote by $\mathcal{D}(a)$ the set of all $\lambda \in \mathbb{C}$ for which

$\text{wind}_\lambda(a) \neq 0$. In plain words $\mathcal{D}(a)$ is the collection of all points trapped by $\mathcal{R}(a)$. In previous works^{17,27,28} it was considered the generating function $a(t) = t^{-1}(1-t)^\alpha g(t)$ satisfying the following properties:

- (i) The constant α belongs to $(0, \infty) \setminus \mathbb{N}$ and $g \in C^\infty(\mathbb{T}) \cap H^\infty$.
- (ii) $g(z) \neq 0$ for $z \in \overline{\mathbb{D}}$, and has an analytic extension to an open neighborhood W of $\mathbb{T} \setminus \{1\}$ not containing the point 1.
- (iii) The range of a is a Jordan curve in \mathbb{C} which is the boundary of a connected region in the complex plane.

When α is an integer number, a becomes a rational function and in such a case, the work of Day¹⁴ assures us non-canonical distribution, property (i) prevents that situation. Let $\lambda_j(T_n(a))$ ($j = 1, \dots, n$) be an ordering of the eigenvalues of $T_n(a)$. For a sufficiently small $\varepsilon > 0$, the eigenvalues $\lambda_j(T_n(a))$ having magnitude larger than ε , are named *inner* while the eigenvalues with magnitude less than or equal to ε are named *extreme*. The authors obtained the following asymptotic inner-eigenvalue expansion,

$$\lambda_j(T_n(a)) = p_0 \left(\omega_n^j \right) + p_1 \left(\omega_n^j \right) \log(n)h + p_2 \left(\omega_n^j \right) h + R \left(\omega_n^j \right),$$

where $h = 1/n$, $\omega_n = \exp(-2i\pi h)$, the coefficients p_0 , p_1 , and p_2 are continuous functions that can be obtained explicitly, and R , being relatively small, plays the role of a remainder term and satisfies the inequality $|R(\omega_n^j)| \leq c(h^{\alpha_0+1} + \log^2(n)h^2)$, with $\alpha_0 = \min\{\alpha, 1\}$ and some constant $c > 0$ depending only on α . It is important to note that an expansion involving only the term p_0 , will produce approximations with errors of order $O(h)$ which coincides with the order that the distance between consecutive eigenvalues have, making the approximation acceptable only for distribution purposes. Hence, in order to obtain acceptable eigenvalue approximations we need an expansion involving at least, the terms p_0 and p_1 . A rather complicated but similar result was obtained²⁹ for a generating function f having several power singularities, that is,

$$f(t) = \frac{1}{t} \prod_{k=1}^K \left(1 - \frac{t}{t_k} \right)^{\alpha_k}, \quad (3)$$

where t_1, \dots, t_K , are distinct points in \mathbb{T} and α_k are positive noninteger constants satisfying $\sum_{k=1}^K \alpha_k < 2$.

Note that a generating function a satisfying the properties (i)–(iii), can be written as

$$a(t) = \frac{1}{t} (1-t)^\alpha g(t) = - \left(1 - \frac{1}{t} \right) (1-t)^{\alpha-1} g(t),$$

and therefore, belongs to the Fisher–Hartwig class (as well as the generating function in (3)). Moreover, it generates a class of Hessenberg Toeplitz matrices stemming from the numerical approximation of certain fractional diffusion equations (FDEs)^{30–32} where the parameter α belongs to the open interval $(0, 2)$. The quoted FDEs with noninteger parameter α have gained a tremendous attention in real world applications,³² because they model anomalous diffusion processes arising in biology, physics, etc.

When a has power singularities over \mathbb{T} , according to Widom,⁷ the spectrum of $T_n(a)$ has canonical distribution, and therefore the respective limiting set $\Lambda(a)$ coincides with the range $\mathcal{R}(a)$. Hence, a belongs to the class \mathcal{T} because $\Lambda(a)$ have one nonclosed analytic arc only. In the mentioned cases, we can verify the canonical distribution by noticing that $p_0(z) = a(z)$.

In asymptotic analysis³³ it is customary to say that a function f admits the asymptotic expansion $\sum_{k=0}^{\infty} a_k(x-x_0)^k$ at x_0 , denoted as

$$f(x) \sim \sum_{k=0}^{\infty} a_k(x-x_0)^k,$$

if we can write $f(x) = \sum_{k=0}^{m-1} a_k(x-x_0)^k + O(|x-x_0|^m)$ for every $m \in \mathbb{Z}_+$. Unfortunately, we have not been able to obtain an asymptotic expansion for an arbitrary non integer α , but since we are mainly interested in the structure of the expansion, we opted to work with a particular value. From this point, fixed a sufficiently small $\varepsilon > 0$ and let $B(0, \varepsilon)$ be the open disk in \mathbb{C} centered at 0 with radius ε . The following is our main result.

Theorem 2. Let a be a generating function satisfying the properties (i)–(iii) and take $\alpha = 3/4$. Then, for every j such that $|\lambda_j(T_n(a))| > \epsilon$, there exists a unique number $t_{j,n}$ satisfying $a(t_{j,n}) = \lambda_j(T_n(a))$ and admitting the following asymptotic expansion

$$t_{j,n} \sim \omega_n^j \left\{ 1 + \sum_{k=1}^{\infty} \sum_{\ell=1}^{N_k} q_k(\omega_n^j) \log^\ell(n) h^{\frac{1}{4}\delta_k} \right\},$$

where

- $\delta_1 = 4, \delta_2 = 7, \delta_3 = 8, \delta_k = 6 + k$ for $k \geq 4$;
- N_k is an integer with $0 \leq N_k \leq \frac{\delta_k}{4}$;
- $h = 1/n$ and $\omega_n \equiv \exp(-2\pi i h)$;
- the coefficients q_k are functions in $C(\mathbb{T})$ depending only on the generating function a .

Our assumptions imply that $T_n(a)$ is a Hessenberg matrix, that is, it can be reached from a lower triangular matrix by adding the diagonal joining the positions $(1, 2)$ with $(n-1, n)$.

To prove Theorem 2, we will use some results from Böttcher et al.,²⁷ which we present here without a proof.

Theorem 3 (Böttcher et al.). Let a be a generating function satisfying the properties (i)–(iii) and take $\lambda \in D(a) \setminus B(0, \epsilon)$.

1. There exists a unique point t_λ in $W \setminus \overline{\mathbb{D}}$ such that $a(t_\lambda) = \lambda$.
2. The determinant of $T_n(a - \lambda)$, denoted as $D_n(a - \lambda)$, can be written as

$$D_n(a - \lambda) = (-1)^n \hat{b}_0^{n+1} \hat{\eta}_n(\lambda),$$

where \hat{b}_0 is the zeroth Fourier coefficient of $b(t) \equiv ta(t) = (1-t)^\alpha g(t)$ and $\hat{\eta}_n(\lambda)$ is the n th Fourier coefficient of the function $\eta(t, \lambda) \equiv 1/\{t(a(t) - \lambda)\}$ with respect to t .

3. We can write

$$\eta(t, \lambda) = \frac{1}{t_\lambda a'(t_\lambda)(t - t_\lambda)} + \psi(t, \lambda),$$

where $\psi(\cdot, \lambda)$ is analytic in W and uniformly bounded in $a(W) \setminus B(0, \epsilon)$, and therefore

$$\hat{\eta}_n(\lambda) = \frac{-1}{t_\lambda^{n+2} a'(t_\lambda)} + \hat{\psi}_n(\lambda),$$

where $\hat{\psi}_n(\lambda)$ is the n th Fourier coefficient of $\psi(\cdot, \lambda)$.

4. As $n \rightarrow \infty$, $\hat{\psi}_n(\lambda)$ admits the expansion

$$\hat{\psi}_n(\lambda) \sim \frac{-1}{\pi} \sum_{r=0}^{\infty} \frac{1}{\lambda^{r+1}} \int_{-\delta}^{\delta} \frac{b^r(e^{i\theta}) \phi(\theta)}{e^{i\theta(n+r+1)}} \theta,$$

where $\delta > 0$ is a small constant with $0 < \epsilon < \delta$, $\phi : \mathbb{R} \rightarrow [0, 1]$ a C^∞ function with support in $[-\delta, \delta]$, and $\phi|_{[-\epsilon, \epsilon]} \equiv 1$.

5. Let $\beta > 0, \delta > 0, v \in C^\infty[0, \delta], v^{(s)}(\delta) = 0$ for all $s \geq 0$. Then, as $n \rightarrow \infty$,

$$\int_0^\delta \theta^{\beta-1} v(\theta) e^{in\theta} \theta \sim \sum_{s=0}^{\infty} \frac{c_s}{n^{s+\beta}},$$

where

$$c_s = \frac{v^{(s)}(0)}{s!} \Gamma(s + \beta) e^{i\frac{\pi}{2}(s+\beta)},$$

and Γ is the usual gamma function.

6. There exists a family of pairwise disjoint sets $\{E_j\}_j$ in \mathbb{C} such that $\omega_n^j \in \partial E_j$ and the eigenvalue relation $D_n(a - \lambda) = D_n(a - a(t_\lambda)) = 0$ has exactly one solution in each E_j .

We will proceed in three steps:

Step 1: For $\lambda \in \mathbb{C}$ we seek an asymptotic expansion for $D_n(a - \lambda)$.

Step 2: We find an implicit equation for the relation $D_n(a - \lambda) = 0$.

Step 3: We use an iterative process to solve the previous relation for λ .

Take $\alpha = 3/4$ and $b(t) \equiv ta(t)$. After a simple calculation we can write

$$b(e^{i\theta}) = (1 - e^{i\theta})^{\frac{3}{4}} g(e^{i\theta}) = e^{-\frac{3i}{8}\pi} \theta^{\frac{3}{4}} g_0(\theta) g(e^{i\theta}),$$

where g_0 is a function belonging to the class $C^\infty[-\delta, \delta]$. It is clear that b has a zero of order $3/4$ at $\theta = 0$. For each $r \in \mathbb{Z}_+$ consider the auxiliary function

$$u_r(\theta) \equiv g_0^r(-\theta) g^r(e^{-i\theta}) \phi(\theta) e^{i\theta(r+1)}, \quad (4)$$

where ϕ is given in part 4 of Theorem 3. The following result gives us an asymptotic expansion for the determinant of $T_n(a - \lambda)$.

Theorem 4. Let a be a generating function satisfying the properties (i)–(iii) and take $\alpha = 3/4$. Then we have

$$D_n(a - \lambda) \sim (-1)^{n+1} \hat{b}_0^{n+1} \left\{ \frac{1}{t_\lambda^{n+2} a'(t_\lambda)} + \frac{1}{\pi} \sum_{r,m=1}^{\infty} \frac{v(r, m)}{\lambda^{r+1}} h^{\frac{1}{4}(3r+4m)} \right\},$$

where $h = 1/n$,

$$v(r, m) \equiv \frac{\Gamma\left(\frac{1}{4}(3r+4m)\right)}{(m-1)!} \Re \left\{ u_r^{(m-1)}(0) e^{\frac{i}{4}\pi(3r+2m)} \right\},$$

$\hat{b}_0 \neq 0$ is the zeroth Fourier coefficient of b , and u_r is given by (4).

Proof. Recall that $\mathcal{D}(a)$ is the set of all complex points trapped by the range of a . By part 4 of Theorem 3 we know that for any $\lambda \in \mathcal{D}(a) \setminus B(0, \epsilon)$, we have

$$D_n(a - \lambda) \sim (-1)^{n+1} \hat{b}_0^{n+1} \left\{ \frac{1}{t_\lambda^{n+2} a'(t_\lambda)} + \frac{1}{\pi} \sum_{r=1}^{\infty} \frac{\xi_n(r)}{\lambda^{r+1}} \right\}, \quad (5)$$

where $\hat{b}_0 \neq 0$ is the zeroth Fourier coefficient of b and

$$\xi_n(r) \equiv \int_{-\delta}^{\delta} \frac{b^r(e^{i\theta}) \phi(\theta)}{e^{i\theta(n+r+1)}} \theta.$$

Now, the expansion

$$\xi_n(r) \sim \sum_{m=1}^{\infty} \frac{\Gamma\left(\frac{1}{4}(3r+4m)\right)}{(m-1)!} \Re \left\{ u_r^{(m-1)}(0) e^{\frac{i}{4}\pi(3r+2m)} \right\} h^{\frac{1}{4}(3r+4m)},$$

where u_r is given by (4), is a consequence of part 5 in Theorem 3. Combining the previous result with (5), we attain

$$D_n(a - \lambda) \sim (-1)^{n+1} \hat{b}_0^{n+1} \left\{ \frac{1}{t_\lambda^{n+2} a'(t_\lambda)} + \frac{1}{\pi} \sum_{r,m=1}^{\infty} \frac{v(r, m)}{\lambda^{r+1}} h^{\frac{1}{4}(3r+4m)} \right\},$$

where

$$v(r, m) \equiv \frac{\Gamma\left(\frac{1}{4}(3r+4m)\right)}{(m-1)!} \Re\left\{u_r^{(m-1)}(0)e^{\frac{i}{4}\pi(3r+2m)}\right\},$$

which proves the assertion of the theorem. ■

We now proceed with the step 2. Solving $D_n(a - \lambda) = 0$ for t_λ^n in Theorem 4, we attain

$$t_\lambda^n \sim \left\{ -\frac{t_\lambda^2 a'(t_\lambda)}{\pi} \sum_{r,m=1}^{\infty} \frac{v(r, m)}{a^{r+1}(t_\lambda)} h^{\frac{1}{4}(3r+4m)} \right\}^{-1},$$

and taking the n th root, for any $j = 0, \dots, n-1$, we reach

$$t_\lambda \sim \omega_n^j \left\{ -\frac{t_\lambda^2 a'(t_\lambda)}{\pi} \sum_{r,m=1}^{\infty} \frac{v(r, m)}{a^{r+1}(t_\lambda)} h^{\frac{1}{4}(3r+4m)} \right\}^{-h}, \quad (6)$$

where $\omega_n = \exp(-2\pi i h)$. To identify the leading term in the previous expression, note that

$$v(1, 1) = \Gamma\left(\frac{7}{4}\right) \Re\left\{u_1(0)e^{\frac{5}{4}i\pi}\right\} = -\frac{g(1)}{\sqrt{2}}\Gamma\left(\frac{7}{4}\right) \neq 0,$$

and rewrite (6) as

$$\begin{aligned} t_\lambda &\sim \omega_n^j \left\{ -\frac{v(1, 1)t_\lambda^2 a'(t_\lambda)}{\pi a^2(t_\lambda)} h^{\frac{7}{4}} \right\}^{-h} \left\{ 1 + \frac{1}{v(1, 1)} \sum_{\substack{r,m=1 \\ (r,m)\neq(1,1)}}^{\infty} \frac{v(r, m)}{a^{r-1}(t_\lambda)} h^{\frac{1}{4}(3r+4m-7)} \right\}^{-h} \\ &= \omega_n^j h^{-\frac{7}{4}h} \left\{ \frac{-\pi a^2(t_\lambda)}{v(1, 1)t_\lambda^2 a'(t_\lambda)} \right\}^h \left\{ 1 + \frac{1}{v(1, 1)} \sum_{\substack{r,m=1 \\ (r,m)\neq(1,1)}}^{\infty} \frac{v(r, m)}{a^{r-1}(t_\lambda)} h^{\frac{1}{4}(3r+4m-7)} \right\}^{-h}. \end{aligned} \quad (7)$$

At this point we have reached an asymptotic expression for t_λ involving h with powers $(3r+4m)/4$, $r, m \geq 1$. To sort those powers we need to calculate first the integer set $S \equiv \{3r+4m : r, m \in \mathbb{Z} \text{ and } r, m \geq 1\}$.

The set S is related to the Frobenius coin problem, that is, given positive integers a_1, a_2, \dots, a_ℓ , such that $\gcd(a_1, a_2, \dots, a_\ell) = 1$, find the largest integer that cannot be expressed as an integer conical combination of these numbers, that is, as a sum $k_1 a_1 + k_2 a_2 + \dots + k_\ell a_\ell$, where k_1, k_2, \dots, k_ℓ , are non-negative integers. The solution for the case $\ell = 2$ is known to be $a_1 a_2 - a_1 - a_2$. But in our case $r, m \geq 1$ while in the Frobenius problem it is $r, m \geq 0$. Nevertheless, we can easily adapt the Frobenius result obtaining

$$S = \{7, 10, 11\} \cup \{s \in \mathbb{N} : s \geq 13\}.$$

Let us order S with the sequence $(\gamma_k)_{k=0}^\infty$, that is, $\gamma_0 = 7$, $\gamma_1 = 10$, $\gamma_2 = 11$, and $\gamma_k = 10 + k$ for $k \geq 3$. We want to emphasize here that each γ_k can be attained by different combinations of r and m , for instance $\gamma_9 = 19 = 3 \cdot 1 + 4 \cdot 4 = 3 \cdot 5 + 1 \cdot 4$.

Therefore, we can rewrite (7) as

$$t_\lambda \sim \omega_n^j n^{\frac{1}{4}\gamma_0 h} p_0^h(t_\lambda) \left\{ 1 + \sum_{k=1}^{\infty} p_k(t_\lambda) h^{\frac{1}{4}(\gamma_k-7)} \right\}^{-h}, \quad (8)$$

where

$$p_0(t_\lambda) \equiv \frac{-\pi a^2(t_\lambda)}{v(1, 1)t_\lambda^2 a'(t_\lambda)} \quad \text{and} \quad p_k(t_\lambda) \equiv \frac{1}{v(1, 1)} \sum_{\ell=1}^{N_k} \frac{v(r_k(\ell), m_k(\ell))}{a^{r_k(\ell)-1}(t_\lambda)} \quad (k \geq 1),$$

and the pairs of numbers $(r_k(1), m_k(1)), \dots, (r_k(N_k), m_k(N_k))$ are the different combinations appearing in S satisfying $3r_k(\ell) + 4m_k(\ell) = \gamma_k$.

By elementary analysis, we reach

$$p_0^h(t_\lambda) = \exp\{h \log(p_0(t_\lambda))\} = 1 + \log(p_0(t_\lambda))h + \frac{1}{2}\log^2(p_0(t_\lambda))h^2 + \dots,$$

and

$$\left\{ 1 + \sum_{k=1}^{\infty} p_k(t_\lambda) h^{\frac{1}{4}(\gamma_k - 7)} \right\}^{-h} = 1 - h \sum_{k=1}^{\infty} p_k(t_\lambda) h^{\frac{1}{4}(\gamma_k - 7)} + \frac{h(h+1)}{2} \left(\sum_{k=1}^{\infty} p_k(t_\lambda) h^{\frac{1}{4}(\gamma_k - 7)} \right)^2 + \dots$$

Hence, after expanding, multiplying, and ordering in (8), we obtain

$$t_\lambda \sim \omega_n^j n^{\frac{7}{4}h} \left\{ 1 + \sum_{k=1}^{\infty} \hat{p}_k(t_\lambda) h^{\frac{1}{4}\delta_k} \right\} \quad (9)$$

where

$$\delta_1 = 4, \quad \delta_2 = 7, \quad \delta_3 = 8, \quad \delta_k = 6 + k \quad (k \geq 4),$$

each \hat{p}_k is a linear combination of some p_k 's, which are functions in $C^\infty(W \setminus \bar{\mathbb{D}})$, that can be determined explicitly.

We are left with the step 3. By part 6 of Theorem 3, we know that there exists a collection of mutually disjoint neighborhoods of each $\omega_n^j, j = 0, \dots, n-1$, containing exactly one solution of (9). We are now ready to prove our main result.

Proof of Theorem 2. Let t_λ be a solution of (9). Since $a(t_\lambda) = \lambda$ is an eigenvalue of $T_n(a)$, we conclude that there are exactly n solutions and we denote them as $t_{j,n} \equiv t_{\lambda_j(T_n(a))}, j = 1, \dots, n$. Now we follow an iterative process over (9). For simplicity, take $u \equiv h^{1/4}$. Using the expansion

$$n^{\frac{7}{4}h} = 1 + \frac{7}{4} \log(n)h + \frac{49}{32} \log^2(n)h^2 + \dots,$$

and multiplying, we reach

$$t_\lambda^{(1)} \equiv \omega_n^j \{1 + O(\log(n)u^4)\} \{1 + O(u^4)\} = \omega_n^j + O(\log(n)u^4),$$

which is our first iteration. We need to iterate once more to understand the general shape. For the second iteration notice that $\hat{p}_j(t_\lambda^{(1)}) = \hat{p}_j(\omega_n^j) + O(\log(n)u^4)$ and write

$$\begin{aligned} t_\lambda^{(2)} &\equiv \omega_n^j \left\{ 1 + \frac{7}{4} \log(n)u^4 + O(\log^2(n)u^8) \right\} \\ &\quad \times \left\{ 1 + \hat{p}_1(\omega_n^j)u^4 + O(\log(n)u^8) + \hat{p}_2(\omega_n^j)u^7 + O(\log(n)u^{11}) \right\} \\ &= \omega_n^j \left\{ 1 + \frac{7}{4} \log(n)u^4 + \hat{p}_1(\omega_n^j)u^4 + \hat{p}_2(\omega_n^j)u^7 + O(\log^2(n)u^8) \right\}. \end{aligned}$$

By continuing this process we finish the theorem. ■

The previous theoretical calculation serves now as an inspiration for the computational part and in particular, with the aid of Theorem 2, we can visualize and formulate the following hypothesis. The argument $\omega_n^j = \exp(\pi i j h)$ can be changed to $\theta_{j,n} = \pi j h$, and the numerical experiments reveal that the terms involving logarithms can be omitted. Notice also that the asymptotic expansion involves powers of h^β with some $\beta \in (0, 1]$ instead of h as appeared in previous works.

2.1 | Working hypothesis

Suppose that $T_n(f)$ are non-Hermitian for every sufficiently large n and $f \in \mathcal{T}$. Then, for some integer $\rho \geq 0$, some $\beta \in (0, 1]$, every n , and every $j = 1, \dots, n$, the following asymptotic expansion holds

$$\begin{aligned}\lambda_j(T_n(f)) &= \mathfrak{f}(\theta_{j,n}) + \sum_{k=1}^{\rho} c_k(\theta_{j,n}) h^{\beta k} + E_{j,n,\rho} \\ &= \mathfrak{f}^R(\theta_{j,n}) + \sum_{k=1}^{\rho} c_k^R(\theta_{j,n}) h^{\beta k} + E_{j,n,\rho}^R \\ &\quad + i \left\{ \mathfrak{f}^I(\theta_{j,n}) + \sum_{k=1}^{\rho} c_k^I(\theta_{j,n}) h^{\beta k} + E_{j,n,\rho}^I \right\}, \\ &= \sum_{k=0}^{\rho} \{c_k^R(\theta_{j,n}) + i c_k^I(\theta_{j,n})\} h^{\beta k} + E_{j,n,\rho},\end{aligned}\tag{10}$$

where:

- the eigenvalues $\lambda_j(T_n(f))$ are arranged from one end of $\mathcal{R}(\mathfrak{f})$ to the other;
- the sequences $\{c_0^R, c_1^R, c_2^R, \dots\}$ and $\{c_0^I, c_1^I, c_2^I, \dots\}$ are functions from $(0, \pi)$ to \mathbb{R} depending only on f , and $\mathfrak{f}^R \equiv c_0^R, \mathfrak{f}^I \equiv c_0^I$;
- $h \equiv 1/(n+1)$ and $\theta_{j,n} \equiv j\pi h$;
- $E_{j,n,\rho} = E_{j,n,\rho}^R + i E_{j,n,\rho}^I = O(h^{\beta(\rho+1)})$ is the remainder (the error) function, which satisfies the inequality $|E_{j,n,\rho}| \leq \kappa h^{\beta(\rho+1)}$ for some constant κ depending only on ρ .

It is worth to mention that we used $h = 1/(n+1)$ instead of $h = 1/n$ for defining the grid $\theta_{j,n}$. This is not a surprise, because for specific classes of matrices it is advantageous to define a different equispaced grid, for example, by choosing $h = 1/(n+1)$ or even $h = 1/(n+2)$: to give a basic example, if we consider real symmetric Toeplitz matrices, then the best grid is obtained by choosing $h = 1/(n+1)$ and the related grid is exact, a “perfect grid,” when the real symmetric Toeplitz matrix is also tridiagonal; see for example, Reference 19 and references therein.

Expansions of the type considered in WH have been formally proven in a number of works. For example, for a real-valued Laurent polynomial satisfying the so-called simple-loop condition, the expansion (10) with $\rho = 2$ and $\beta = 1$ was obtained.³⁴ For real-valued generating functions belonging to the weighted Wiener algebra W^γ with $\gamma \geq 4$, and satisfying the so-called *simple-loop* condition, the same was proved with $\rho = 4$ and $\beta = 1$.¹⁷ With some additional hypothesis, the same expansion was obtained for $\gamma \geq 2$ with $\rho = \lfloor \gamma \rfloor$ and $\beta = 1$.²⁸ For complex-valued symbols having a power singularity, an expansion similar to (10) was obtained with $\rho = 2$ and $\beta = 1/4$.²⁷ Böttcher et al.²⁹ extended these results to generating functions having a finite number of power singularities. Recent investigations,^{35,36} also obtained similar expansions.

In fact, it was conjectured¹⁹ that the simple-loop assumptions can be relaxed and reduced only to the monotonicity of the generating function.

Ekström and Vassalos¹⁶ considered the real-valued case using a similar WH with the sole difference that ρ could be taken arbitrarily large. Barrera et al.³⁵ proved that this is true only for $\beta = 1$ and $\rho \leq 3$ and false in general. But interestingly, the asymptotic expansion with three terms is good enough to compute the eigenvalues until machine-precision (double precision) even for moderately “small” matrices. Hence we adjusted WH to agree with the existing theory.

For notational purposes, since we typically have two different expansions for \mathfrak{f}^R and \mathfrak{f}^I , we introduce $\xi_{j,n}^R$ and $\xi_{j,n}^I$ denoting two “perfect grids,” that is, two grids satisfying

$$\lambda_j(T_n(f)) = \mathfrak{f}^R(\xi_{j,n}^R) + i \mathfrak{f}^I(\xi_{j,n}^I) \quad \text{for } j = 1, \dots, n.$$

Typically, they are not equispaced and known only in very few situations, that is, tridiagonal or circulant Toeplitz matrices.

Asymptotic expansions of such nonregular grids were discussed for matrix sequences $\{T_n(f)\}_n$ with real eigenvalues.³⁷ We want to emphasize that finding an asymptotic expansion for $\xi_{j,n}^{\Re}$ or $\xi_{j,n}^{\Im}$ is equivalent to working with the expansion

$$\lambda_j(T_n(f)) = \mathfrak{f} \left(\theta_{j,n} + \sum_{k=1}^{\rho} r_k(\theta_{j,n}) h^{\beta k} + E_{j,n,\rho} \right).$$

This approach is included formally in the simple-loop method (see e.g., References 17 and 34 and the recent numerical version³⁸). In the current paper the grids $\xi_{j,n}^{\Re}$ and $\xi_{j,n}^{\Im}$ are numerically approximated, and are only used for visualization.

3 | MOTIVATION AND ILLUSTRATIVE EXAMPLES

In this section we present four examples supporting WH, but how can an example support WH? Well, we need to present generating functions f in the class \mathcal{T} such that the eigenvalues of $T_n(f)$ satisfy the expansion (10). For that purpose, let

$$\lambda_j^{\text{NA}(\rho)}(T_n(f)) \equiv \sum_{k=0}^{\rho-1} c_k(\theta_{j,n}) h^{\beta k},$$

be the approximation of the eigenvalue $\lambda_j(T_n(f))$ through the ρ terms expansion proposed in WH which is defined later in detail in Algorithm 1 of Section 4. For testing the accuracy of our results we introduce the following notation for the individual and maximum errors:

$$\begin{aligned} E_{j,n}^{\text{NA}(\rho)}(f) &\equiv |\lambda_j(T_n(f)) - \lambda_j^{\text{NA}(\rho)}(T_n(f))|, \\ E_n^{\text{NA}(\rho)}(f) &\equiv \max \left\{ E_{j,n}^{\text{NA}(\rho)}(f) : j = 1, \dots, n \right\}. \end{aligned} \quad (11)$$

To test WH, the key point is that, for each generating function f , (10) implies that $E_n^{\text{NA}(\rho)}(f) = O(h^{\beta\rho})$ for some constants ρ and β , that is, the normalized maximum errors $(n+1)^{\beta\rho} E_n^{\text{NA}(\rho)}(f)$ must remain bounded as n increases.

In the following examples, in Section 5, we will provide error tables where this behavior can be noted. The precise calculation of those errors, obviously involves the precise calculation of the respective eigenvalues. Hence we briefly recall the fact that standard double precision eigenvalue solvers (such as, `Eigenvalues` in MATHEMATICA, `eig` in MATLAB, and `eigvals` in JULIA³⁹) fail to give accurate eigenvalues of certain matrices $T_n(f)$; see, for example, References 16, 24, 40, and 41. High precision computations, using packages such as `GENERICLINEARALGEBRA.JL` in JULIA, can approximate the eigenvalues, but they are very expensive from the computational point of view. Therefore, approximating \mathfrak{f} , and c_1, c_2, \dots , on the grid $\theta_{j,n}$, and using matrix-less methods to approximate the spectrum of $T_n(f)$, for large n , can be computationally advantageous.

In the present article we used the software JULIA with data types `Float64` (standard double precision) and `BigFloat` (128, 256, 512, and 1024 bit). `Float64` corresponds approximately to 53 bit `BigFloat`, so when stating 53 bit, we mean standard double precision. Machine epsilon for the different data types are of the order 10^{-16} (`Float64`) and $10^{-38}, 10^{-77}, 10^{-154}, 10^{-308}$ (`BigFloat`), respectively. Numerical experiments were conducted on a computer with an AMD Ryzen Threadripper 3970X CPU (256 GB RAM) and with JULIA version 1.7.2.

Recall that $\mathcal{ER}(f)$ stands for the essential range of f . The following is a short summary of the considered examples:

- **Example 1:** $T_n(f)$ is a nonsymmetric complex tridiagonal matrix, $\mathfrak{f} \neq f$, and \mathfrak{f} is known. The eigenvalues $\lambda_j(T_n(f))$ are known explicitly. $\mathbb{C} \setminus \mathcal{ER}(f)$ is formed by two connected components (i.e., $\mathcal{ER}(f)$ disconnects the complex plane) and the limiting set $\Lambda(f)$ has one nonclosed analytic arc;
- **Example 2:** $T_n(f)$ is a complex symmetric pentadiagonal matrix, and $\mathfrak{f} = f$. The eigenvalues $\lambda_j(T_n(f))$ are not known explicitly. $\mathbb{C} \setminus \mathcal{ER}(f)$ is connected (i.e., $\mathcal{ER}(f)$ does not disconnect the complex plane) and the limiting set $\Lambda(f)$ has one nonclosed analytic arc;
- **Example 3:** $T_n(f)$ is a complex symmetric heptadiagonal matrix, and $\mathfrak{f} = f$. The eigenvalues $\lambda_j(T_n(f))$ are not known explicitly. $\mathbb{C} \setminus \mathcal{ER}(f)$ is connected (i.e., $\mathcal{ER}(f)$ does not disconnect the complex plane) and the limiting set $\Lambda(f)$ has one nonclosed analytic arc.

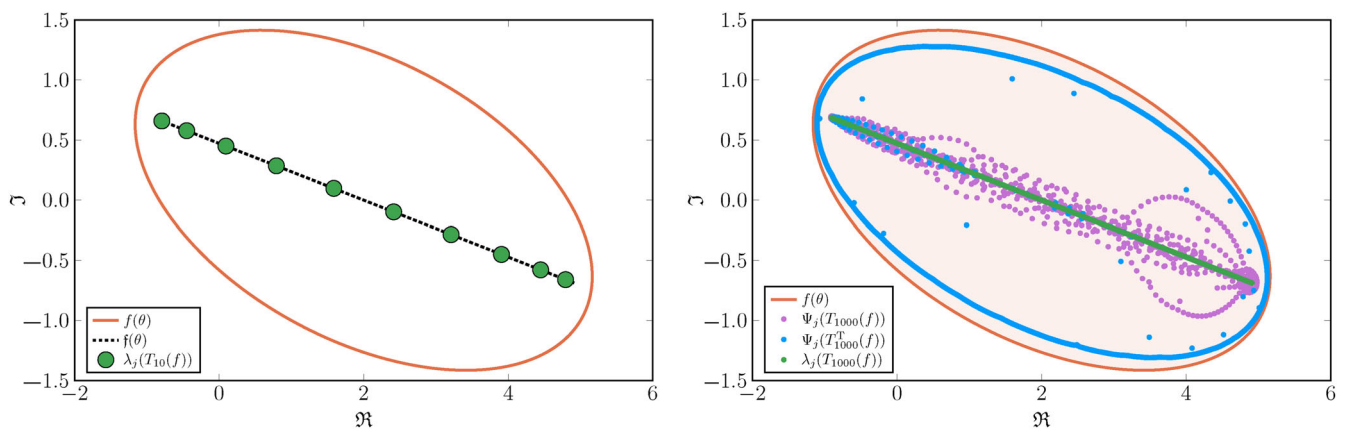


FIGURE 1 [Example 1: generating function $f(\theta) = (-2 + i)e^{-i\theta} + 2 - e^{i\theta}$] Left: generating function f (red line), symbol \mathfrak{f} (black dashed line), and eigenvalues $\lambda_j(T_n(f)) = \lambda_j(T_n(\mathfrak{f}))$ for $n = 10$ (green dots). Right: Convex hull of the generating function f (light red), the numerically computed eigenvalues $\Psi_j(T_n(f))$, $\Psi_j(T_n^T(f))$ (using double precision), and $\lambda_j(T_n(f)) = \lambda_j(T_n(\mathfrak{f})) = \mathfrak{f}(\theta_{j,n})$ (using, respectively, 128 bit BigFloat, double precision, or (14) with (12)), for $n = 1000$.

TABLE 1 [Example 1: generating function $f(\theta) = (-2 + i)e^{-i\theta} + 2 - e^{i\theta}$] Errors $\epsilon_{p,n}(f)$, see (15), for the eigenvalues $\lambda_j(T_n(f))$ computed with precision P_p , where $P = (53, 128, 256, 512)$ and $p = 1, \dots, 4$.

<i>n</i>	53	128	256	512
101	10^{-7}	10^{-35}	10^{-74}	10^{-150}
203	10^{-1}	10^{-34}	10^{-73}	10^{-150}
407	10^{-1}	10^{-34}	10^{-73}	10^{-149}
815	10^{-1}	10^{-34}	10^{-72}	10^{-149}
1631	10^{-1}	10^{-32}	10^{-71}	10^{-149}

- **Example 4:** $T_n(f)$ is a nonsymmetric complex tetradiagonal matrix, $\mathfrak{f} \neq f$, and \mathfrak{f} is unknown. The eigenvalues $\lambda_j(T_n(f))$ are not known explicitly. $\mathbb{C} \setminus \mathcal{ER}(f)$ is formed by two connected components (i.e. $\mathcal{ER}(f)$ disconnects the complex plane) and the limiting set $\Lambda(f)$ has one nonclosed analytic arc.

In Section 5 we perform numerical experiments in relation with Examples 5–8 (extending the corresponding Examples 1–4).

Example 1. Ekström and Vassalos¹⁶ studied the spectrum for the generating function $f(\theta) = -2e^{-i\theta} + 2 - e^{i\theta}$, which produces a tridiagonal Toeplitz matrix $T_n(f)$ that has a real spectrum described by the symbol $\mathfrak{f}(\theta) = 2 - 2\sqrt{2}\cos(\theta)$. The exact eigenvalues of $T_n(f)$ are given by $\lambda_j(T_n(f)) = \lambda_j(T_n(\mathfrak{f})) = \mathfrak{f}(\theta_{j,n})$, where the sampling grid is

$$\theta_{j,n} = \frac{\pi j}{n+1} = \pi j h, \quad j = 1, \dots, n. \quad (12)$$

Now, consider instead the generating function

$$f(\theta) = (-2 + i)e^{-i\theta} + 2 - e^{i\theta} = f^R(\theta) + i f^I(\theta), \quad (13)$$

where

$$f^R(\theta) = 2 + \sin(\theta) - 3\cos(\theta) \quad \text{and} \quad f^I(\theta) = \sin(\theta) + \cos(\theta).$$

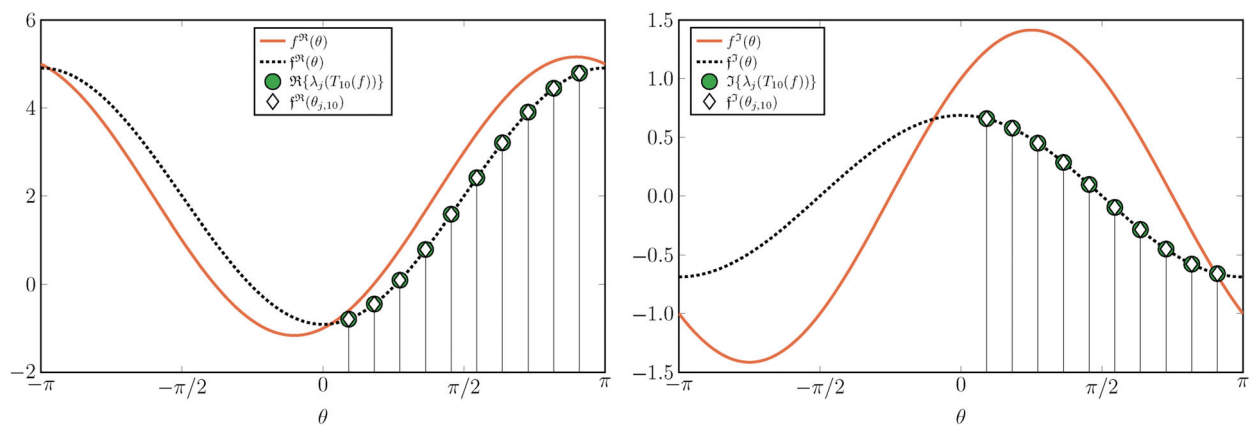


FIGURE 2 [Example 1: generating function $f(\theta) = (-2 + i)e^{-i\theta} + 2 - e^{i\theta}$] Left: The real part of the generating function f (red line), the symbol \hat{f}^R (black dashed line), the real part of the eigenvalues of $T_{10}(f)$ (green dots), and the sampling of \hat{f}^R on the grid (12) (white diamonds). Right: The corresponding imaginary counterparts of the left panel.

In this case $T_n(f)$, is a tridiagonal Toeplitz matrix and its eigenvalues can be exactly calculated (see Reference 2 Ch. 2). The corresponding symbol \hat{f} that describes the complex-valued spectrum of $T_n(f)$ (see Reference 16 Eq. 4) is

$$\begin{aligned}\hat{f}(\theta) &= \hat{f}_0 + \sqrt{\hat{f}_1 \sqrt{\hat{f}_{-1}}} \cos(\theta) \\ &= 2 + 2i\sqrt{-2+i} \cos(\theta) \\ &= \hat{f}_0 + 2\hat{f}_{\pm 1} \cos(\theta) \\ &= \hat{f}_0 + 2\hat{f}_{\pm 1}^R \cos(\theta) + 2i\hat{f}_{\pm 1}^I \cos(\theta),\end{aligned}\quad (14)$$

where $\hat{f}_0 = 2$ and

$$\hat{f}_{\pm 1} = \sqrt[4]{5} \left\{ -\cos\left(\frac{1}{2} \arctan\left(\frac{1}{2}\right)\right) + i \sin\left(\frac{1}{2} \arctan\left(\frac{1}{2}\right)\right) \right\} = \hat{f}_{\pm 1}^R + i\hat{f}_{\pm 1}^I.$$

The eigenvalues of $T_n(f)$ (and $T_n(\hat{f})$) are given by (14) using the grid (12). Moreover, we have

$$T_n(f) = \begin{bmatrix} 2 & -2+i & & & \\ -1 & 2 & -2+i & & \\ & \ddots & \ddots & \ddots & \\ & & -1 & 2 & -2+i \\ & & & -1 & 2 \end{bmatrix},$$

and

$$\begin{aligned}T_n(\hat{f}) &= \begin{bmatrix} 2\hat{f}_{-1} & & & \\ \hat{f}_1 2 & \hat{f}_{-1} & & \\ & \ddots & \ddots & \\ & & \hat{f}_1 2 & \hat{f}_{-1} \\ & & \hat{f}_1 & 2 \end{bmatrix} = \begin{bmatrix} 2 & \hat{f}_{-1}^R & & & \\ \hat{f}_1^R & 2 & \hat{f}_{-1}^R & & \\ & \ddots & \ddots & \ddots & \\ & & \hat{f}_1^R & 2 & \hat{f}_{-1}^R \\ & & & \hat{f}_1^R & 2 \end{bmatrix} \\ &+ i \begin{bmatrix} 0 & \hat{f}_{-1}^I & & & \\ \hat{f}_1^I & 0 & \hat{f}_{-1}^I & & \\ & \ddots & \ddots & \ddots & \\ & & \hat{f}_1^I & 0 & \hat{f}_{-1}^I \\ & & & \hat{f}_1^I & 0 \end{bmatrix}.\end{aligned}$$

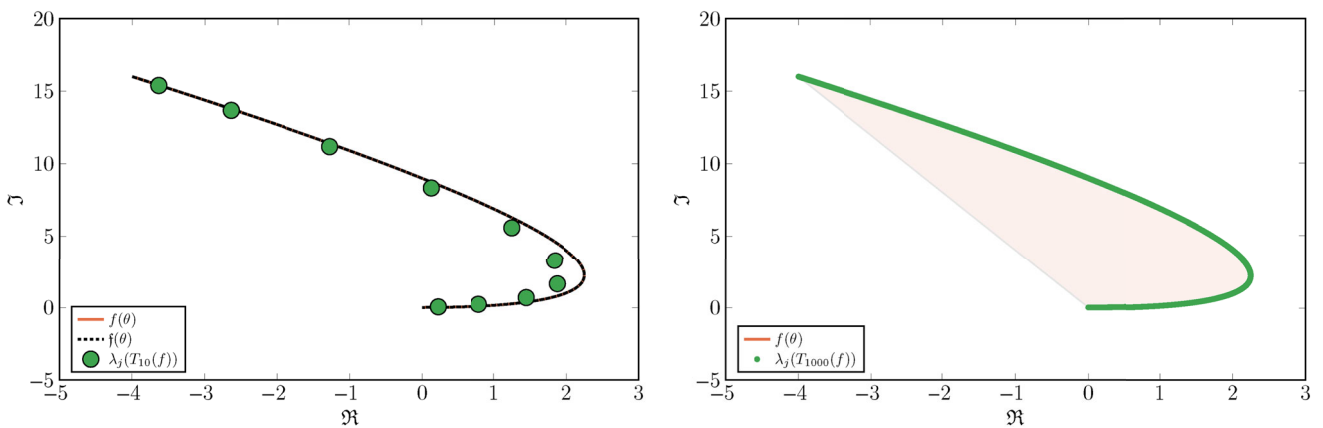


FIGURE 3 [Example 2: generating function $f(\theta) = 2 \cos(\theta) - 2 \cos(2\theta) + i(2 - 2 \cos(\theta))^2$] Left: generating function $f = \mathfrak{f}$ (red line and black dashed line) and $\lambda_j(T_{10}(f))$ (green dots). Right: The generating function f (red line), its convex hull (light red), and the eigenvalues $\lambda_j(T_{1000}(f))$ (green dots).

In the left panel of Figure 1 we show the functions f (red line) and \mathfrak{f} (black dashed line), and the eigenvalues $\lambda_j(T_n(f)) = \lambda_j(T_n(\mathfrak{f}))$ (green dots) for $n = 10$. In the right panel of Figure 1 we show the function f (red line) and its convex hull (light red shaded region). The numerically (double precision) computed eigenvalues $\Psi_j(T_n(f))$ (pink dots) and $\Psi_j(T_n^T(f))$ (blue dots), for $n = 1000$, are shown. These numerically computed eigenvalues Ψ_j are related to the pseudo-spectrum, discussed for example in References 1, 24, 40, and 41. Furthermore, the true eigenvalues $\lambda_j(T_n(f)) = \lambda_j(T_n(\mathfrak{f})) = \mathfrak{f}(\theta_{j,n})$ (green dots) are shown. The numerical computation of the eigenvalues $\lambda_j(T_n(f))$ required a high precision computation (for example, 128 bit BigFloat), whereas for $\lambda_j(T_n(\mathfrak{f}))$ standard double precision was enough. Also, the exact expression for the eigenvalues is given by sampling (14) with the grid (12).

In order to determine the numerical precision needed to calculate the “exact” eigenvalues, we introduce the errors

$$\epsilon_{p,n}(f) \equiv \max\{|\lambda_{j,p+1}(T_n(f)) - \lambda_{j,p}(T_n(f))| : j = 1, \dots, n\}, \quad (15)$$

where $\lambda_{j,p}(T_n(f))$ stands for the j th eigenvalue of the matrix $T_n(f)$ calculated with a precision of P_p bits and where P is the sequence $P = (53, 128, 256, 512, 1024)$. Table 1 shows the data and, for a given precision P_p , the errors are of approximately the same order regardless of n , and then 128 bit computations are enough for $O(10^{-16})$ accuracy (double precision).

In Figure 2 we present the real (left panel) and imaginary (right panel) parts of the spectrum of $T_n(f)$. For $n = 10$ we see that the eigenvalues are equispaced samplings of \mathfrak{f}^R and \mathfrak{f}^I . We present the eigenvalues on the grid (12) since both \mathfrak{f}^R and \mathfrak{f}^I are even functions (whereas neither the real nor the imaginary parts of f are even).

Example 2. In this example we construct a function that generates complex-valued pentadiagonal matrices. The function is chosen to be

$$\begin{aligned} f(\theta) &= (i-1)e^{-2i\theta} + (1-4i)e^{-i\theta} + 6i + (1-4i)e^{i\theta} + (i-1)e^{2i\theta} \\ &= \mathfrak{f}^R(\theta) + i\mathfrak{f}^I(\theta) = \mathfrak{f}(\theta). \end{aligned} \quad (16)$$

where

$$\begin{aligned} \mathfrak{f}^R(\theta) &= 2 \cos(\theta) - 2 \cos(2\theta), \\ \mathfrak{f}^I(\theta) &= 6 - 8 \cos(\theta) + 2 \cos(2\theta) = (2 - 2 \cos(\theta))^2. \end{aligned}$$

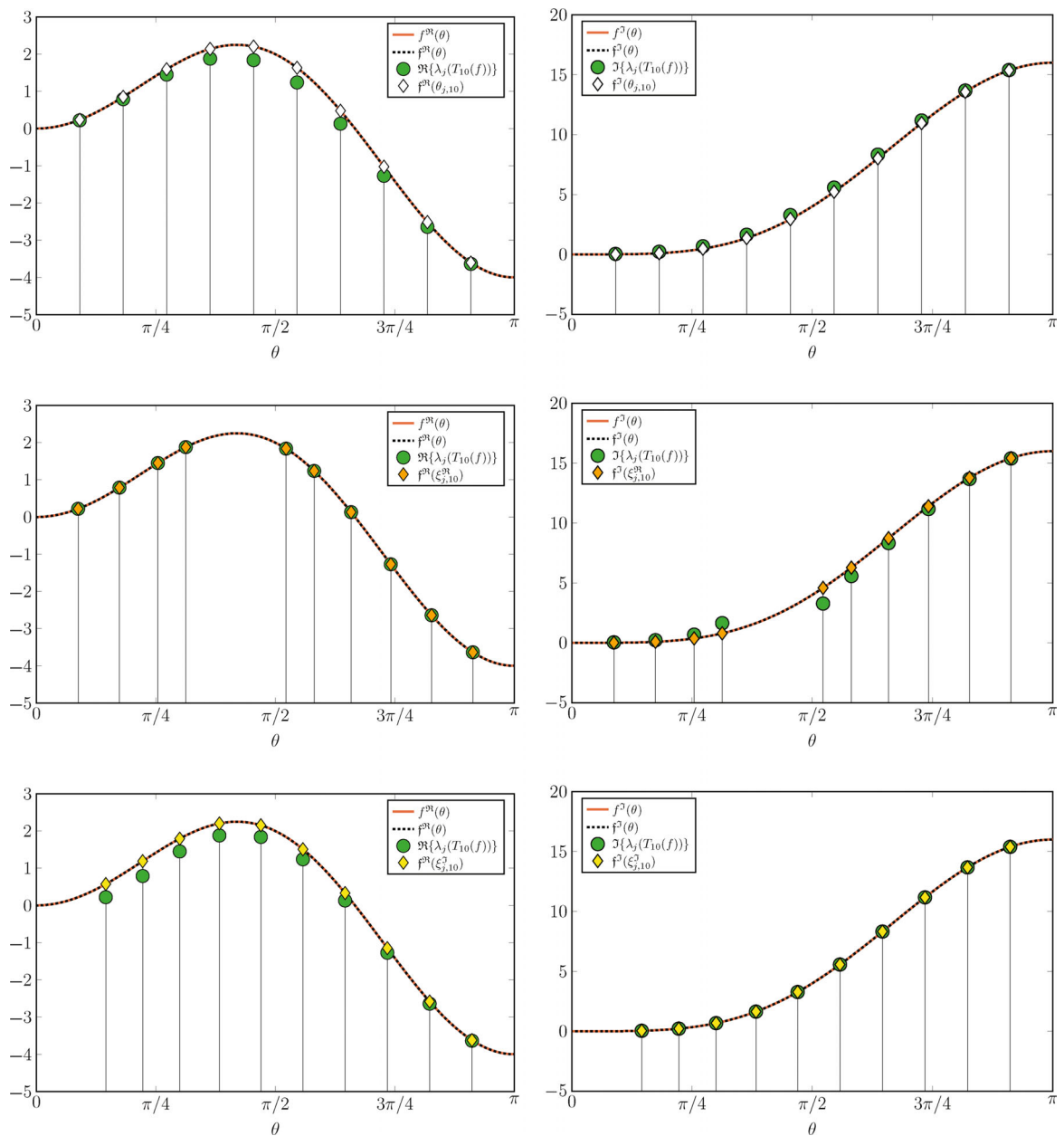


FIGURE 4 [Example 2: generating function $f(\theta) = 2 \cos(\theta) - 2 \cos(2\theta) + i(2 - 2 \cos(\theta))^2$] Left: real part of the generating function f (red line) and $\mathfrak{f}^R = \Re\{f\}$ (black dashed line). Eigenvalues $\lambda_j(T_{10}(f))$, and sampling grids $\theta_{j,n}$ (top), $\xi_{j,n}^R$ (middle), and $\xi_{j,n}^I$ (bottom). Right: Imaginary counterparts of the left panels.

Thus, we have $T_n(f) = T_n(\mathfrak{f}^R) + i T_n(\mathfrak{f}^I)$, where

$$T_n(\mathfrak{f}^R) = \begin{bmatrix} 0 & 1 & -1 & & & \\ 1 & 0 & 1 & -1 & & \\ -1 & 1 & 0 & 1 & -1 & \\ \ddots & \ddots & \ddots & \ddots & \ddots & \\ & -1 & 1 & 0 & 1 & -1 \\ & & -1 & 1 & 0 & 1 \\ & & & -1 & 1 & 0 \end{bmatrix}, \quad T_n(\mathfrak{f}^I) = \begin{bmatrix} 6 & -4 & 1 & & & \\ -4 & 6 & -4 & 1 & & \\ 1 & -4 & 6 & -4 & 1 & \\ \ddots & \ddots & \ddots & \ddots & \ddots & \\ & 1 & -4 & 6 & -4 & 1 \\ & & 1 & -4 & 6 & -4 \\ & & & 1 & -4 & 6 \end{bmatrix}.$$

The spectra of the generated Toeplitz matrices $T_n(f)$ are complex-valued.

In this example we have $f = \mathfrak{f}$. As it can be observed in Figure 3, there are no numerical issues in computing the spectrum of $T_n(f)$ using double precision, and as expected the spectrum converges, in the Hausdorff metric, to the range $\mathcal{R}(f)$ as n increases.

In Figure 4 we present the spectrum of $T_n(f)$, for $n = 10$, with different sampling grids $\theta_{j,n}$ (top), $\xi_{j,n}^{\Re}$ (middle), and $\xi_{j,n}^{\Im}$ (bottom). The left panels concern the real part of the spectrum of $T_n(f)$ and the right panels the imaginary part.

The top panels of Figure 4 show that there exists an error in the eigenvalue approximations, when sampling the function \mathfrak{f} using the grid $\theta_{j,10}$, defined in (12), both in the real (left panel) and the imaginary (right panel) parts of the spectrum. In the middle panels of Figure 4 we use the perfect grid $\xi_{j,10}^{\Re}$ for sampling \mathfrak{f} , that is, we obtain an exact representation of the real part of the spectrum. However, the imaginary part of the spectrum is not exact. The bottom panels of Figure 4 show the results when sampling \mathfrak{f} with the perfect grid $\xi_{j,10}^{\Im}$. The left panel shows the erroneous approximated real part and the right panel shows the exact imaginary part of the spectrum of $T_{10}(f)$.

Example 3. In this example we construct the following complex-valued function,

$$\begin{aligned} f(\theta) &= -i e^{-3i\theta} + (i-1)e^{-2i\theta} + e^{-i\theta} + e^{i\theta} + (i-1)e^{2i\theta} - i e^{3i\theta} \\ &= \underbrace{2 \cos(\theta) - 2 \cos(2\theta)}_{=\mathfrak{f}^{\Re}(\theta)} + \underbrace{i(2 \cos(2\theta) - 2 \cos(3\theta))}_{=\mathfrak{f}^{\Im}(\theta)} = \mathfrak{f}(\theta), \end{aligned} \quad (17)$$

which generates matrices with complex spectra.

We have $T_n(f) = T_n(\mathfrak{f}^{\Re}) + i T_n(\mathfrak{f}^{\Im})$, where

$$T_n(\mathfrak{f}^{\Re}) = \begin{bmatrix} 01 & -1 & & & & & & & \\ 10 & 1-1 & & & & & & & \\ -11 & 01 & -1 & & & & & & \\ -1 & 10 & 1-1 & & & & & & \\ \ddots & \ddots & \ddots & \ddots & & & & & \\ & & -1 & 10 & 1-1 & & & & \\ & & & -11 & 01 & -1 & & & \\ & & & & -1 & 10 & 1 & & \\ & & & & & -11 & 0 & & \end{bmatrix},$$

$$T_n(\mathfrak{f}^{\Im}) = \begin{bmatrix} 0 & 0 & 1 & -1 & & & & & \\ 0 & 0 & 0 & 1 & -1 & & & & \\ 1 & 0 & 0 & 0 & 1 & -1 & & & \\ -1 & 1 & 0 & 0 & 0 & 1 & -1 & & \\ \ddots & & \\ & & -1 & 1 & 0 & 0 & 0 & 1 & -1 \\ & & & -1 & 1 & 0 & 0 & 0 & 1 \\ & & & & -1 & 1 & 0 & 0 & 0 \\ & & & & & -1 & 1 & 0 & 0 \end{bmatrix}.$$

In Figures 5 and 6 we present the same information as in Figures 3 and 4 in Example 2, but for (17).

Inspecting the distribution of the eigenvalues in Figure 6, for the “perfect grids” (middle left and bottom right panels), we note that there are “distinct grids” between the points where the derivative of the symbols are zero. See a similar behavior in the middle left panel of Figure 4 of Example 2. This observation leads to the conjecture that for real-valued nonmonotone symbols an avenue of research is to use matrix-less methods

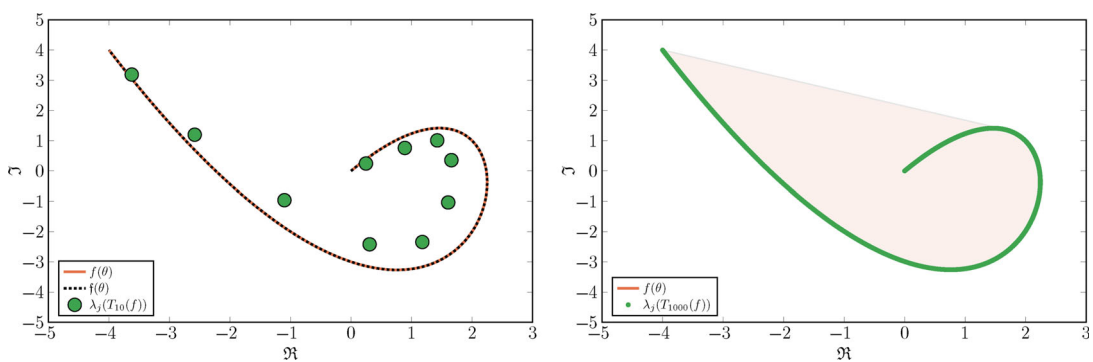


FIGURE 5 [Example 3: generating function $f(\theta) = 2 \cos(\theta) - 2 \cos(2\theta) + i(2 \cos(2\theta) - 2 \cos(3\theta))$] Left: generating function f (red line), symbol $\mathfrak{f} = f$ (black dashed line), and $\lambda_j(T_{10}(f))$ (green dots). Right: generating function f (red line), with its convex hull (light red), and $\lambda_j(T_{1000}(f))$ (green dots).

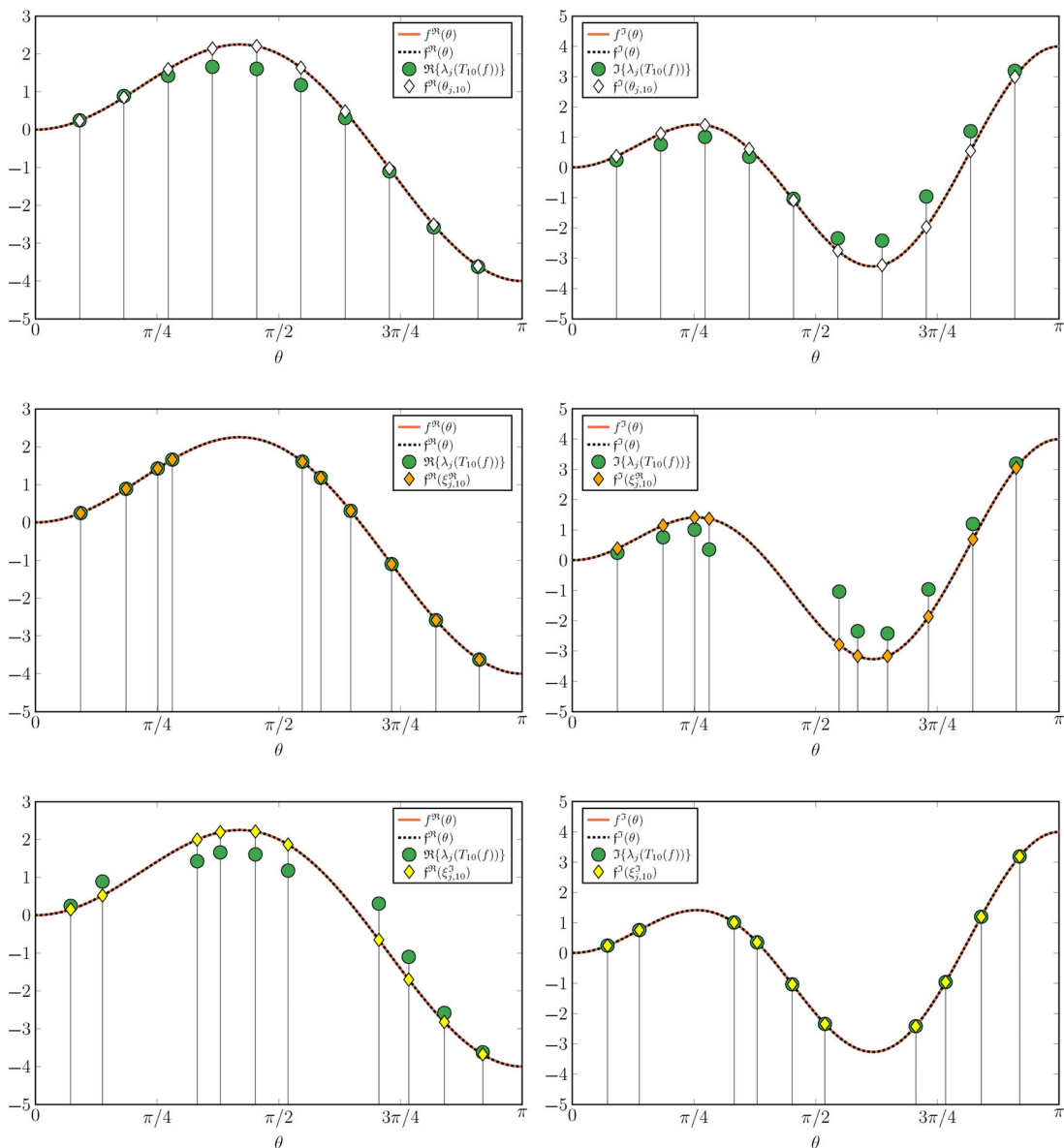


FIGURE 6 [Example 3: generating function $f(\theta) = 2 \cos(\theta) - 2 \cos(2\theta) + i(2 \cos(2\theta) - 2 \cos(3\theta))$] Left: Real part of the generating function $f(\theta)$ (red line) and $\mathfrak{f}^R = \Re\{f\}$ (black dashed line). Eigenvalues $\lambda_j(T_{10}(f))$, and sampling grids $\theta_{j,n}$ (top), $\xi_{j,n}^R$ (middle), and $\xi_{j,n}^I$ (bottom). Right: imaginary counterparts of the left panels.

locally between all the points in $[-\pi, \pi]$ where the derivative of the symbols is zero. In this way we could theoretically obtain a finite number of different grids (or sub-generating functions with their separate asymptotic expansions), and then reconstruct the full spectrum.

Example 4. In this example we consider the generating function

$$f(\theta) = e^{2i\theta} + ce^{i\theta} + ce^{-i\theta}, \quad (18)$$

where c is a complex constant. In this case the symbol \mathfrak{f} is unknown exactly but we can approximate it numerically with the Algorithm 2, which we will explain in Section 4.2. Let $\tilde{\mathfrak{f}}$ be its numerical approximation.

This generating function was studied by Böttcher et al.,¹⁵ where an asymptotic eigenvalue expansion was obtained. The authors gave a nice description of the respective limiting set depending on the parameter c , which can have 1, 2, or 3 analytic arcs. We here selected two values of c that will produce a limiting set with one arc only. The respective Toeplitz matrix $T_n(f)$ is a tetra-diagonal matrix given by

$$T_n(f) = \begin{bmatrix} 0 & c & & & \\ c & 0 & c & & \\ 1 & c & 0 & c & \\ \ddots & \ddots & \ddots & \ddots & \\ & 1 & c & 0 & c \\ & & 1 & c & 0 \end{bmatrix}.$$

Let γ be the piece of the curve $\{z \in \mathbb{C} : |1+z| = 2|z|^2\}$ lying in the closed disk $\{z \in \mathbb{C} : |1+z| \leq 1\}$, and let Ω be the bounded region in the complex plane with boundary

$$\left\{ \pm 2 \frac{(1+z+z^2)^{\frac{3}{2}}}{z(1+z)} : z \in \gamma \right\}.$$

Then if $c \notin \Omega$ we know¹⁵ that the limiting set consists of two (smoothly connected) analytic arcs. In this example we studied the cases $c = 6$ and $c = 3 + i$. See Figures 7–10. When $c = 6$ the limiting set $\Lambda(f)$ is a real segment and hence \mathfrak{f} is real valued.

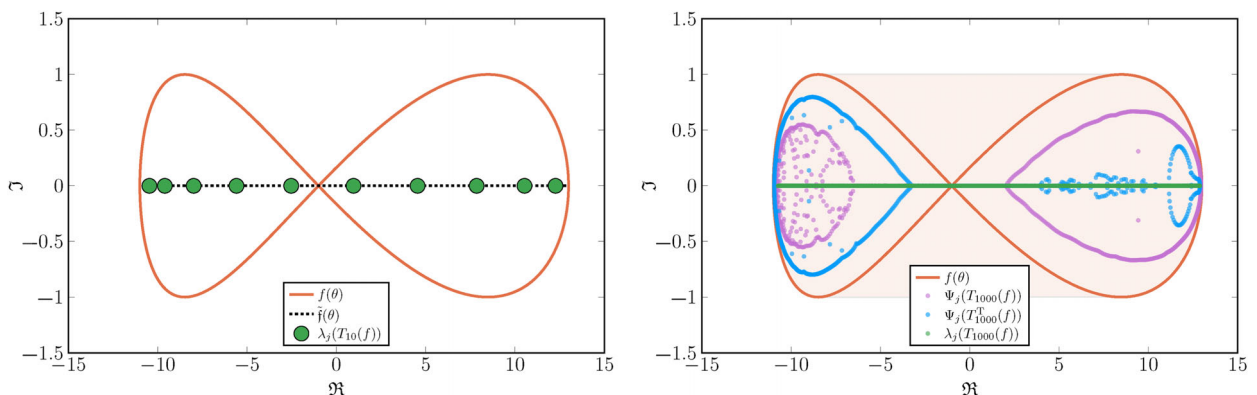


FIGURE 7 [Example 4: generating function $f(\theta) = e^{2i\theta} + ce^{i\theta} + ce^{-i\theta}$ with $c = 6$] Left: generating function f (red line), symbol \mathfrak{f} (black dashed line), and $\lambda_j(T_{10}(f))$ (green dots). Right: Convex hull of the generating function f (light red), the numerically computed eigenvalues $\Psi_j(T_n(f))$, $\Psi_j(T_n^T(f))$ (using double precision), and $\lambda_j(T_n(f)) = \lambda_j(T_n(\mathfrak{f})) = \mathfrak{f}(\theta_{j,n})$ (using respectively 1024 bit BigFloat, double precision, or (18) with (12)), for $n = 1000$.

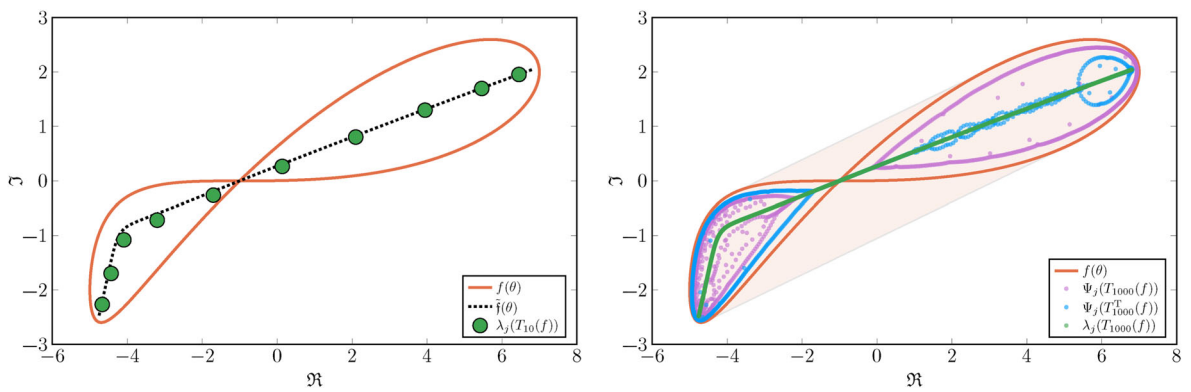


FIGURE 8 [Example 4: generating function $f(\theta) = e^{2i\theta} + ce^{i\theta} + ce^{-i\theta}$] The same as Figure 7 with $c = 3 + i$.

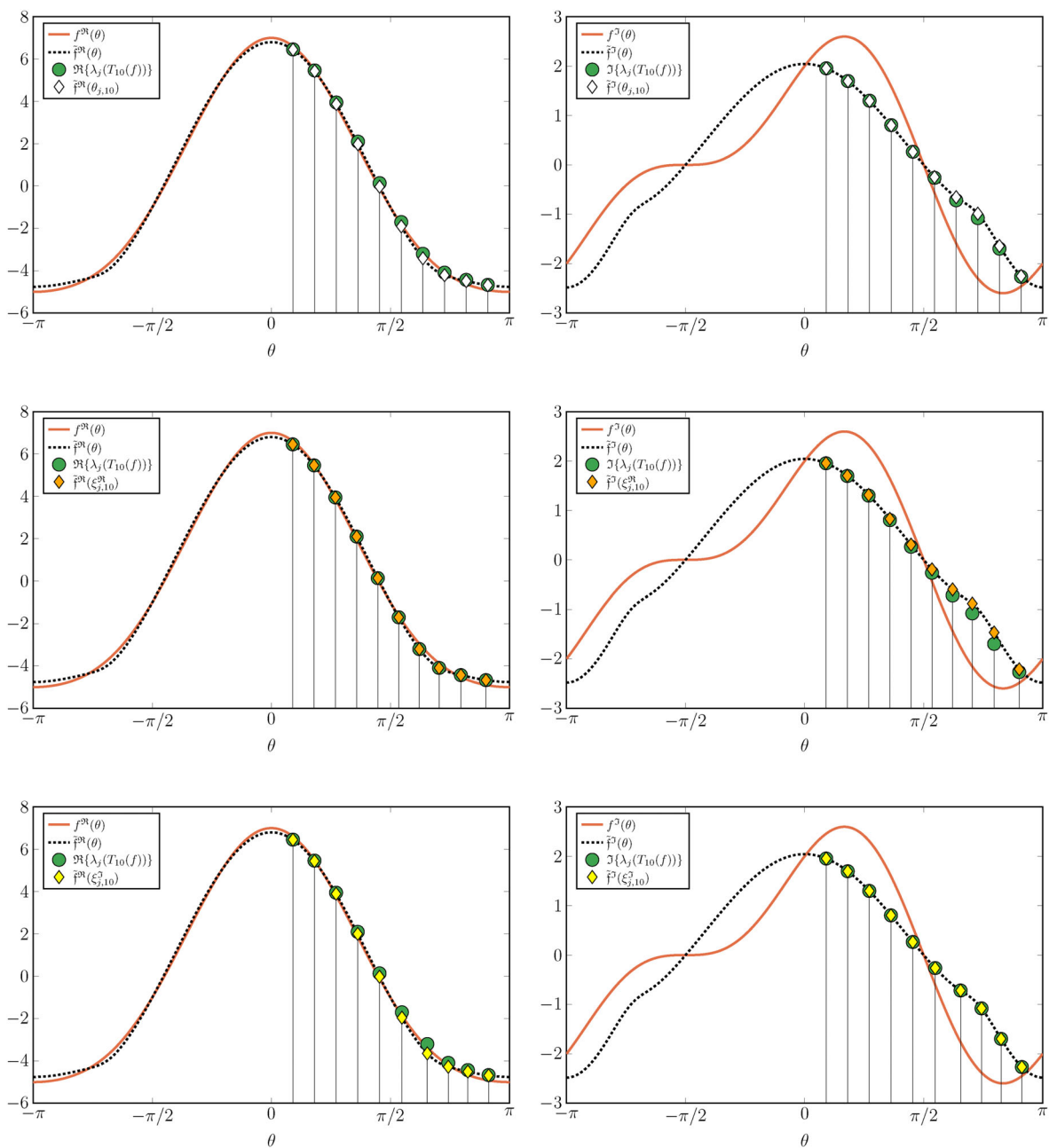


FIGURE 9 [Example 4: generating function $f(\theta) = e^{2i\theta} + ce^{i\theta} + ce^{-i\theta}$] The same as Figure 10 with $c = 3 + i$.

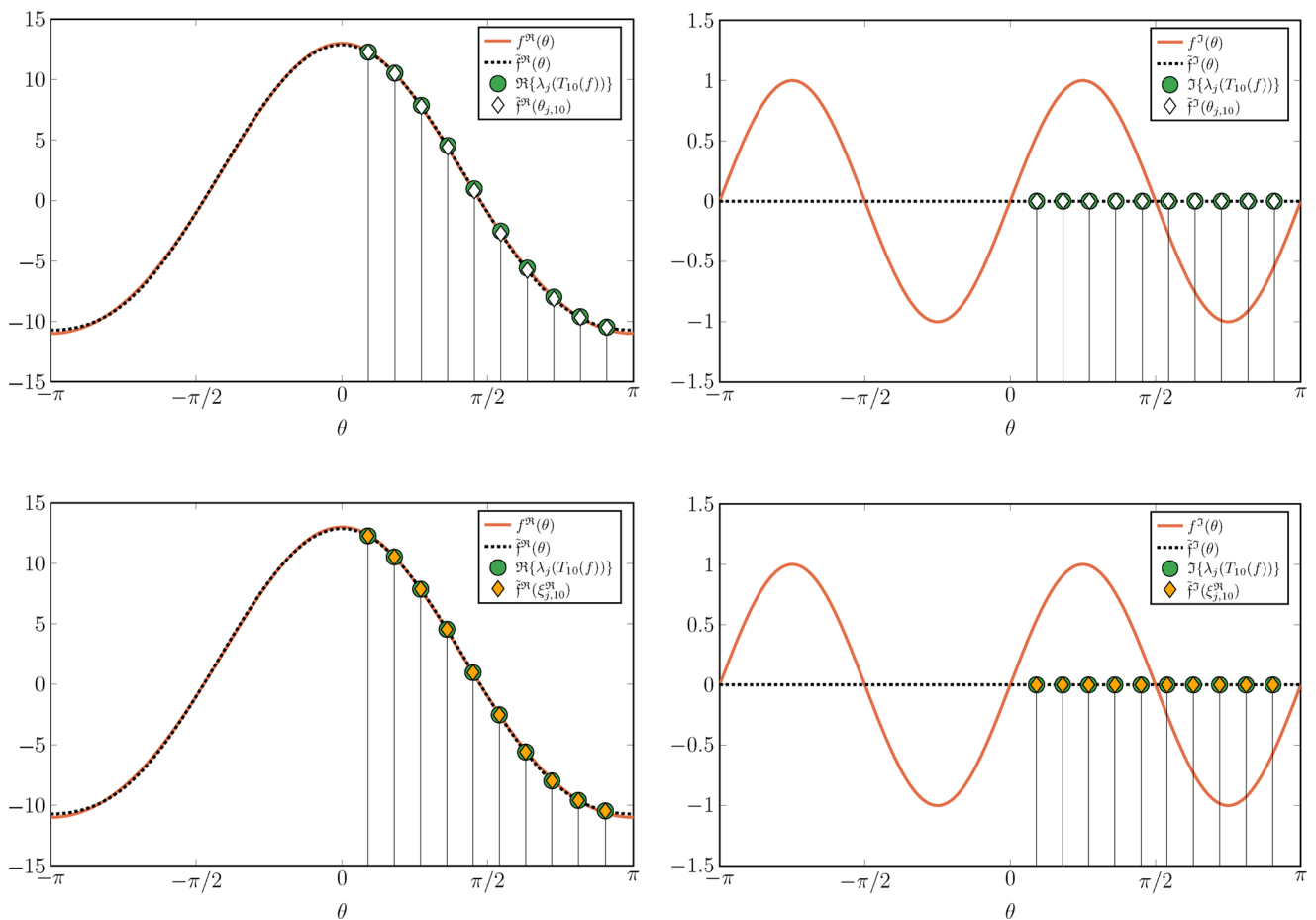


FIGURE 10 [Example 4: generating function $f(\theta) = e^{2i\theta} + ce^{i\theta} + ce^{-i\theta}$ with $c = 6$] Left: Real part of the generating function f (red line) and $\mathfrak{f}^{\Re} = \Re\{f\}$ (black dashed line). Eigenvalues $\lambda_j(T_{10}(f))$, and sampling grids $\theta_{j,n}$ (top) and $\xi_{j,n}^{\Re}$ (bottom). Since $\mathfrak{f}^{\Im} = 0$ we do not approximate a $\xi_{j,n}^{\Im}$. Right: imaginary counterparts of the left panels.

4 | THE ALGORITHM

We introduce a new matrix-less method to accurately approximate the expansion functions c_k^{\Re}, c_k^{\Im} , for $k = 0, \dots, \rho$, where we recall that $c_0^{\Re} \equiv \mathfrak{f}^{\Re}$ and $c_0^{\Im} \equiv \mathfrak{f}^{\Im}$. We note that Algorithm 1 is a further modified and extended version of Alg. 1 in Reference ,16 which differs from just treating the real and imaginary parts separately. Here we introduce an “eigenvalue function,” `eig_fun`, as a “black box” argument, to accommodate customized ordering for more general spectra. The use of the proposed idea can be applied to more complicated symbols and matrices; for example, preconditioning, block matrices generated by matrix-valued symbols, boundary conditions, inclusion of small-norm matrices, and matrices from problems with variable coefficients. Subsequently, in Section 4.2 we present the procedure (same as Alg. 2 in Reference 16) to obtain the symbol \mathfrak{f} by approximating its Fourier series.

4.1 | Approximating the expansion functions c_k^{\Re} and c_k^{\Im}

We refer the reader to the following papers, and the references therein, for the details on the *matrix-less* methods, and the asymptotic expansion of eigenvalues using the spectral symbol; Böttcher et al. ¹⁵ on the limiting set, Böttcher et al. ³⁴, Bogoya et al. ^{17,28} and Batalshchikov et al. ¹⁸ on sequences generated by simple-loop symbols, Barrera et al. ³⁵ and Ekström et al. ¹⁹ on the asymptotic expansion of eigenvalues for Hermitian sequences (preconditioned ²⁰, block-banded ²¹, parallel ²² and IgA ²³). Ekström and Vassalos ¹⁶ extended these methods so that it is no longer required to have the spectral symbol as an input argument in the algorithms.

Algorithm 1. Approximate the expansion functions c_k^{\Re} and c_k^{\Im} for $k = 0, \dots, \rho$, on the grid θ_{j,n_0}

```

using LinearAlgebra, GenericLinearAlgebra
setprecision(BigFloat, 128)
function compute_c(n0:: Integer, alpha:: Integer, eig_fun:: Function, T:: DataType)
    """
    Return C (alpha+1 \times n0) with approximated samplings of c_k(theta_{j, n0})
    for k=0, ..., alpha, theta_{j, n0}=j\pi/(n0+1), and j=1, ..., n0.
    eig_fun returns ordered eigenvalues for the matrix sequence, for a given size and data type.
    T is the data type, e.g., Complex{Float64} or Complex{BigFloat}.

    # Example
    C = compute_c(100, 3, eig_fun_example_1_and_5, Complex{BigFloat})
    """

    j0 = 1:n0
    E = zeros(T, alpha+1, n0)
    hs = zeros(real(T), alpha+1)
    for kk = 0:alpha
        nk = (2^kk)*(n0+1)-1
        jk = (2^kk)*j0
        hs[kk+1] = convert(real(T), 1)/(nk+1)
        E[kk+1, :] = eig_fun(nk, T)[jk]
    end
    V = zeros(T, alpha+1, alpha+1)
    for ii = 0:alpha, jj = 0:alpha
        V[ii+1, jj+1] = hs[ii+1]^jj
    end
    return C=V\E
end

```

Assuming that the complex eigenvalues of the matrices $T_n(f)$ admit an asymptotic expansion in terms of an unknown (or known) function $f = f^{\Re} + if^{\Im}$ instead of f (or $f = \tilde{f}$), as in WH (10), we can use Algorithm 1 in order to find approximations of both f and the functions c_k^{\Re}, c_k^{\Im} with the following formula,

$$\begin{aligned}\lambda_j(T_{n_0}(f)) &\approx \sum_{k=0}^{\rho} \left\{ \tilde{c}_k^{\Re}(\theta_{j,n_0}) h_0^k + i \tilde{c}_k^{\Im}(\theta_{j,n_0}) h_0^k \right\} \\ &= \underbrace{\tilde{f}^{\Re}(\theta_{j,n_0}) + i \tilde{f}^{\Im}(\theta_{j,n_0})}_{=\tilde{f}(\theta_{j,n_0})} + \sum_{k=1}^{\rho} \left\{ \tilde{c}_k^{\Re}(\theta_{j,n_0}) h_0^k + i \tilde{c}_k^{\Im}(\theta_{j,n_0}) h_0^k \right\},\end{aligned}\quad (19)$$

where the approximations \tilde{c}_k^{\Re} and \tilde{c}_k^{\Im} (where $\tilde{f}^{\Re} \equiv \tilde{c}_0^{\Re}$ and $\tilde{f}^{\Im} \equiv \tilde{c}_0^{\Im}$) are obtained from $\rho+1$ small matrices $T_{n_0}(f), \dots, T_{n_\rho}(f)$. The approximation of the eigenvalues of $T_n(f)$, for arbitrary $n \gg n_0$, can be derived by using (19) and the interpolation-extrapolation technique previously used by Ekström and Garoni,²² once for the real and once for the imaginary part of the eigenvalues. In the following Algorithm 1 we show an implementation in JULIA of the algorithm that computes $\tilde{c}_k^{\Re}(\theta_{j,n_0})$ and $\tilde{c}_k^{\Im}(\theta_{j,n_0})$ for $k = 0, \dots, \rho$. The input arguments are $n_0, \rho, \text{eig_fun}$, and the data type of computation T ; the algorithm is written for clarity and not for performance.

4.2 | Approximating the function f from \tilde{c}_0^{\Re} and \tilde{c}_0^{\Im}

We here assume, for the sake of simplicity, that the sought functions f^{\Re} and f^{\Im} are real-valued and even, so that we have cosine Fourier series of the form

$$\begin{aligned}f^{\Re}(\theta) &= \hat{f}_0^{\Re} + 2 \sum_{k=1}^{\infty} \hat{f}_k^{\Re} \cos(k\theta), \quad \hat{f}_k^{\Re} \in \mathbb{R}, \\ f^{\Im}(\theta) &= \hat{f}_0^{\Im} + 2 \sum_{k=1}^{\infty} \hat{f}_k^{\Im} \cos(k\theta), \quad \hat{f}_k^{\Im} \in \mathbb{R}.\end{aligned}$$

As we shall see in Examples 5–7, if \mathfrak{f}^{\Re} and \mathfrak{f}^{\Im} are real cosine trigonometric polynomials, then we are able to recover the exact expression of \mathfrak{f} up to machine precision; otherwise, as in Example 8, we will get a truncated representation of the Fourier series of \mathfrak{f} . More specifically, what we do is the following: for each $j = 1, \dots, n_0$, we consider the approximations $\tilde{c}_0^{\Re}(\theta_{j,n_0})$ and $\tilde{c}_0^{\Im}(\theta_{j,n_0})$ provided by Algorithm 1 and approximate the first n_0 Fourier coefficients $\hat{f}_0^{\Re}, \dots, \hat{f}_{n_0-1}^{\Re}$ and $\hat{f}_0^{\Im}, \dots, \hat{f}_{n_0-1}^{\Im}$ with the numbers $\tilde{f}_0^{\Re}, \dots, \tilde{f}_{n_0-1}^{\Re}$ and $\tilde{f}_0^{\Im}, \dots, \tilde{f}_{n_0-1}^{\Im}$, respectively, obtained by solving the following two linear systems

$$\begin{aligned}\tilde{f}_0^{\Re} + 2 \sum_{k=1}^{n_0-1} \tilde{f}_k^{\Re} \cos(k\theta_{j,n_0}) &= \tilde{c}_0^{\Re}(\theta_{j,n_0}), \\ \tilde{f}_0^{\Im} + 2 \sum_{k=1}^{n_0-1} \tilde{f}_k^{\Im} \cos(k\theta_{j,n_0}) &= \tilde{c}_0^{\Im}(\theta_{j,n_0}).\end{aligned}$$

The approximated Fourier coefficients and Fourier series of $\mathfrak{f} = \mathfrak{f}^{\Re} + i\mathfrak{f}^{\Im}$ can then, for example, be used to approximate samplings of the function \mathfrak{f} ; as for computing the perfect grids $\xi_{j,n}^{\Re}$ and $\xi_{j,n}^{\Im}$ used for visualization. For code, see Alg. 2 in Reference ,16 and apply it on the real and imaginary parts separately.

5 | NUMERICAL EXAMPLES

To highlight the applicability of the approach and the validity of WH (10), we now employ the proposed Algorithms 1 and 2 (together with Reference 16, Alg 2) on the matrix sequences $\{T_n(f)\}_n$ related to the generating functions discussed in Examples 1–4. To avoid notation crossover, we rename them as Examples 5–8, respectively.

- Example 5: $f \neq \mathfrak{f}$. Since $\mathfrak{f}(\theta_{j,n})$ gives exactly the eigenvalues of $T_n(f)$, only $\mathfrak{f} = \tilde{c}_0$ is nonzero. The function \mathfrak{f} is constructed to machine precision;
- Example 6: $f = \mathfrak{f} = c_0^{\Re} + ic_0^{\Im}$. The approximations \tilde{c}_k^{\Re} and \tilde{c}_k^{\Im} , for $k = 0, \dots, 4$, are computed accurately. The function \mathfrak{f} is constructed to machine precision;
- Example 7: $f = \mathfrak{f} = c_0^{\Re} + ic_0^{\Im}$. The approximations \tilde{c}_k^{\Re} and \tilde{c}_k^{\Im} , for $k = 0, \dots, 3$, are computed accurately. The function \mathfrak{f} is constructed to machine precision.
- Example 8: $f \neq \mathfrak{f}$. The approximations \tilde{c}_k^{\Re} and \tilde{c}_k^{\Im} , for $k = 0, 1$, are computed accurately. The function \mathfrak{f} is constructed to machine precision.

Example 5. We consider again the generating function (13) in Example 1, and use the proposed Algorithm 1. First we define the eigenvalue function `eig_fun` named `eig_fun_example_1_and_5`, which is used as the third argument in Algorithm 1.

Algorithm 2. Compute approximations \tilde{f}_k of the Fourier coefficients \hat{f}_k of \mathfrak{f} , for $k = 0, \dots, n_0 - 1$

```
# Example:
function compute_fourier_coefficients(c0:: Array{T,1}) where T is the data type
"""
Return fourier_coefficients with approximattions of the Fourier coefficients
\mathfrak{f}_k, k=0, ..., n_0-1

# Example
fourier_coefficients_Re = compute_fourier_coefficients(real.(C[1,:]))
"""
n0 = length(c0)
t = LinRange(convert(T,pi)/(n0+1), n0*convert(T,pi)/(n0+1), n0)
F = zeros(T, n0, n0)
F[:,1] = ones(T, n0)
for jj = 2:n0
    F[:,jj] = 2*cos.((jj-1)*t)
end
return fourier_coefficients = F
```

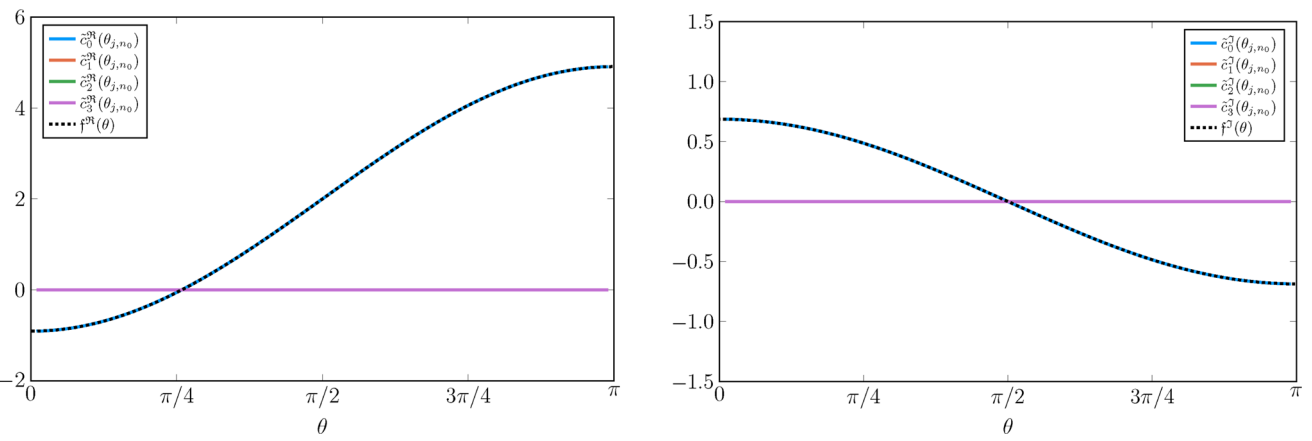


FIGURE 11 [Example 5: generating function $f(\theta) = (-2 + i)e^{-i\theta} + 2 - e^{i\theta}$] Left: The computed $\tilde{c}_k^R(\theta_{j,n_0})$, $k = 0, \dots, \rho$, with $(n_0, \rho) = (101, 4)$ (128 bit) using Algorithm 1. Only $\tilde{c}_0^R(\theta_{j,n_0})$ is nonzero, and matches $f^R(\theta_{j,n_0})$ defined in (14). Right: The corresponding $\tilde{c}_k^I(\theta_{j,n_0})$.

The two arguments are the size n and the data type of the generated matrix, of which the eigenvalues are computed. We here assume that we do not know the symbol \mathfrak{f} . A floating point precision of 128 bit is required, as seen in Table 1; here we use `Complex{BigFloat}`, in order to obtain the correct eigenvalue approximation for the matrices $T_{n_k}(f)$ (assuming a desired accuracy to be at least roughly machine epsilon of double precision, i.e., 10^{-16}). The eigenvalues are arranged in increasing order of the real part using the following JULIA code,

```
function eig_fun_example_1_and_5(n:: Integer, T:: DataType)
    vc = convert.(T, [2+0im, -1+0im])
    vr = convert.(T, [2+0im, -2+1im])
    Tn = toeplitz(n, vc, vr)
    eTn = eigvals(Tn)
    p = sortperm(real.(eTn))
    return eTn[p]
end
```

In Figure 11 we present the approximations \tilde{c}_k^R (left panel) and \tilde{c}_k^I (right panel), $k = 0, \dots, \rho$, $(n_0, \rho) = (101, 4)$ (128 bit). According to the data, the only non-zero \tilde{c}_k^R and \tilde{c}_k^I are the first functions \tilde{c}_0^R and \tilde{c}_0^I , which is expected since the exact eigenvalues of $T_n(f)$ are given by $\mathfrak{f}(\theta_{j,n}) = c_0^R(\theta_{j,n}) + ic_0^I(\theta_{j,n})$.

Example 6. We here return to the generating function (16) in Example 2. The eigenvalues are arranged in increasing order of the imaginary part. Double precision is enough for this example. In Figure 12 we show in the left panel the approximated expansion functions $\tilde{c}_k^R(\theta_{j,n_0})$ for $k = 0, \dots, \rho$, computed using $(n_0, \rho) = (100, 4)$. We see that $\tilde{c}_0^R(\theta_{j,n_0})$ (blue line) and $\mathfrak{f}^R(\theta) = f^R(\theta)$ (black dashed line) overlap. In the right panel we present the corresponding functions $\tilde{c}_k^I(\theta_{j,n_0})$. The terms \tilde{c}_k^I for $k > 0$ do not exactly match the expansion functions \tilde{c}_k if only computing the expansion for the matrix sequence $\{T_n(6 - 8 \cos(\theta) + 2 \cos(2\theta))\}_n$; for example, shown in Reference 42, Fig 2.1.3 and 16, Fig 10. We recover, to machine precision, the nonzero Fourier coefficients $\hat{\mathfrak{f}}_{\pm 1}^R = 1$, $\hat{\mathfrak{f}}_{\pm 2}^R = -1$, $\hat{\mathfrak{f}}_0^R = 6$, $\hat{\mathfrak{f}}_{\pm 1}^I = -4$, and $\hat{\mathfrak{f}}_{\pm 2}^I = 1$.

Figure 13 and Table 2 show the individual and maximum errors $E_{j,n}^{\text{NA}(\rho)}(f)$ (see (11)). Figure 13 shows, in particular, how the error decreases when considering additional terms. The constant behavior of the normalized errors $(n+1)^\rho E_n^{\text{NA}(\rho)}(f)$ in Table 2 proves the applicability of WH (10) until, at least, the fifth term, in this case.

Example 7. In this example we continue the investigation of the generating function in (17) from Example 3. The eigenvalues are ordered as described in Example 3. Double precision is enough for this example. In Figure 14 we show the approximated expansion functions \tilde{c}_k^R (left panels) and \tilde{c}_k^I (right panels) for $(n_0, \rho) = (100, 4)$. The two bottom panels show a close-up of the expansion functions, and as expected, Algorithm 1

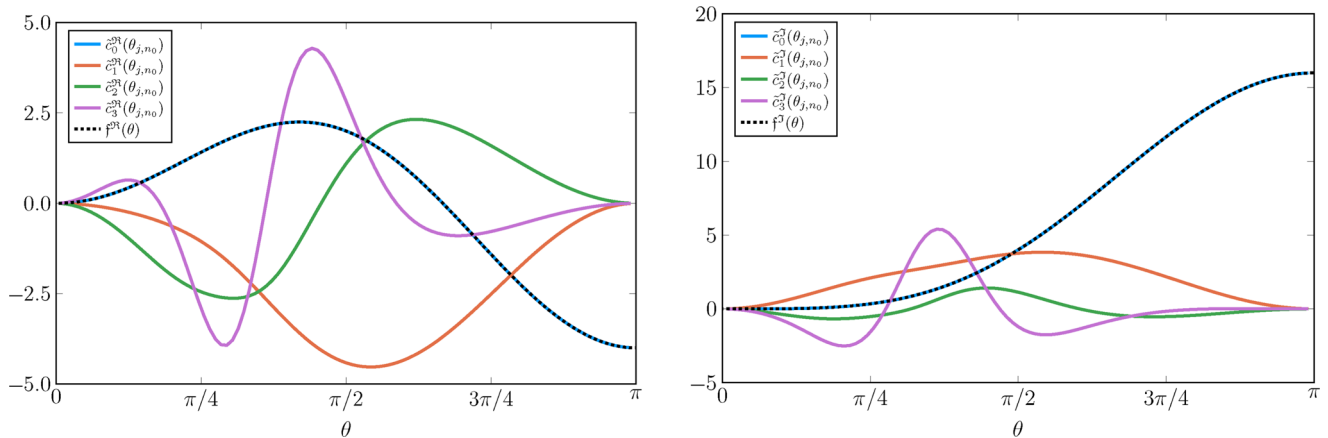


FIGURE 12 [Example 6: generating function $f(\theta) = 2 \cos(\theta) - 2 \cos(2\theta) + i(6 - 8 \cos(\theta) + 2 \cos(2\theta))$] Left: The computed $\tilde{c}_k^R(\theta_{j,n_0})$, $k = 0, \dots, \rho$, with $(n_0, \rho) = (101, 3)$ (53 bit) using Algorithm 1. Right: The corresponding $\tilde{c}_k^I(\theta_{j,n_0})$ as in the left panel.

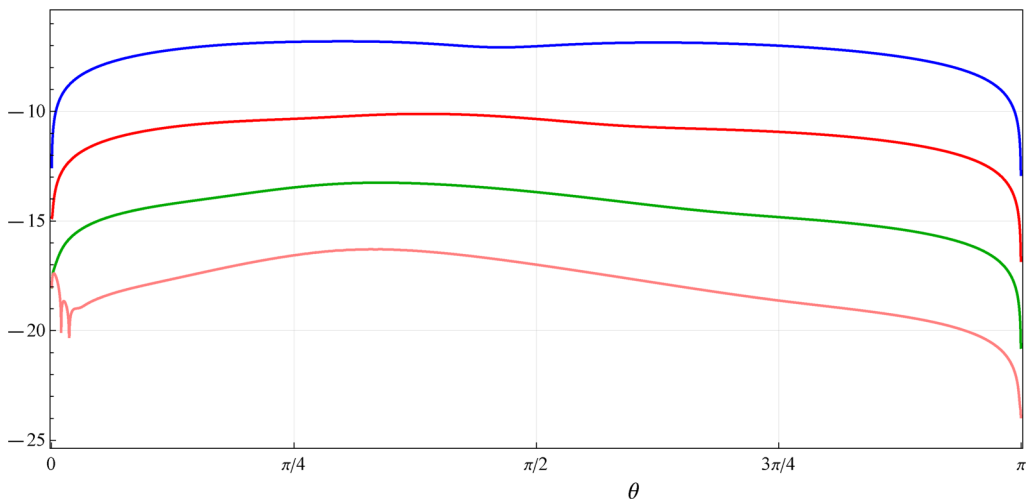


FIGURE 13 [Example 6: generating function $f(\theta) = 2 \cos(\theta) - 2 \cos(2\theta) + i(6 - 8 \cos(\theta) + 2 \cos(2\theta))$] For Algorithm 1, the base 10 logarithm of the individual eigenvalue errors $E_{j,n}^{NA(\rho)}$ for the Toeplitz matrix $T_n(f)$ with $n = 4096$ and different values of ρ : $\rho = 2$ (blue), $\rho = 3$ (red), $\rho = 4$ (green), and $\rho = 5$ (pink).

TABLE 2 [Example 6: generating function $f(\theta) = 2 \cos(\theta) - 2 \cos(2\theta) + i(6 - 8 \cos(\theta) + 2 \cos(2\theta))$] The maximum eigenvalue errors $E_n^{NA(\rho)}$ for the Toeplitz matrix $T_n(f)$, with different matrix sizes n and number of terms $\rho = 1, \dots, 5$.

n	256	512	1024	2048	4096
$E_n^{NA(1)}$	1.6117×10^{-2}	8.0902×10^{-3}	4.0531×10^{-3}	2.0286×10^{-3}	1.0148×10^{-3}
$(n+1)E_n^{NA(1)}$	4.1420×10^0	4.1503×10^0	4.1544×10^0	4.1565×10^0	4.1576×10^0
$E_n^{NA(2)}$	4.0014×10^{-5}	1.0041×10^{-5}	2.5119×10^{-6}	6.2838×10^{-7}	1.5712×10^{-7}
$(n+1)^2 E_n^{NA(2)}$	2.6429×10^0	2.6424×10^0	2.6391×10^0	2.6382×10^0	2.6373×10^0
$E_n^{NA(3)}$	3.1276×10^{-7}	3.9203×10^{-8}	4.9071×10^{-9}	6.1381×10^{-10}	7.6753×10^{-11}
$(n+1)^3 E_n^{NA(3)}$	5.3090×10^0	5.2926×10^0	5.2844×10^0	5.2804×10^0	5.2783×10^0
$E_n^{NA(4)}$	3.6527×10^{-9}	2.2864×10^{-10}	1.4304×10^{-11}	8.9507×10^{-13}	5.5954×10^{-14}
$(n+1)^4 E_n^{NA(4)}$	1.5935×10^1	1.5835×10^1	1.5789×10^1	1.5777×10^1	1.5765×10^1
$E_n^{NA(5)}$	5.2602×10^{-11}	1.6569×10^{-12}	5.1962×10^{-14}	1.6246×10^{-15}	5.1318×10^{-17}
$(n+1)^5 E_n^{NA(5)}$	5.8975×10^1	5.8869×10^1	5.8790×10^1	5.8675×10^1	5.9238×10^1

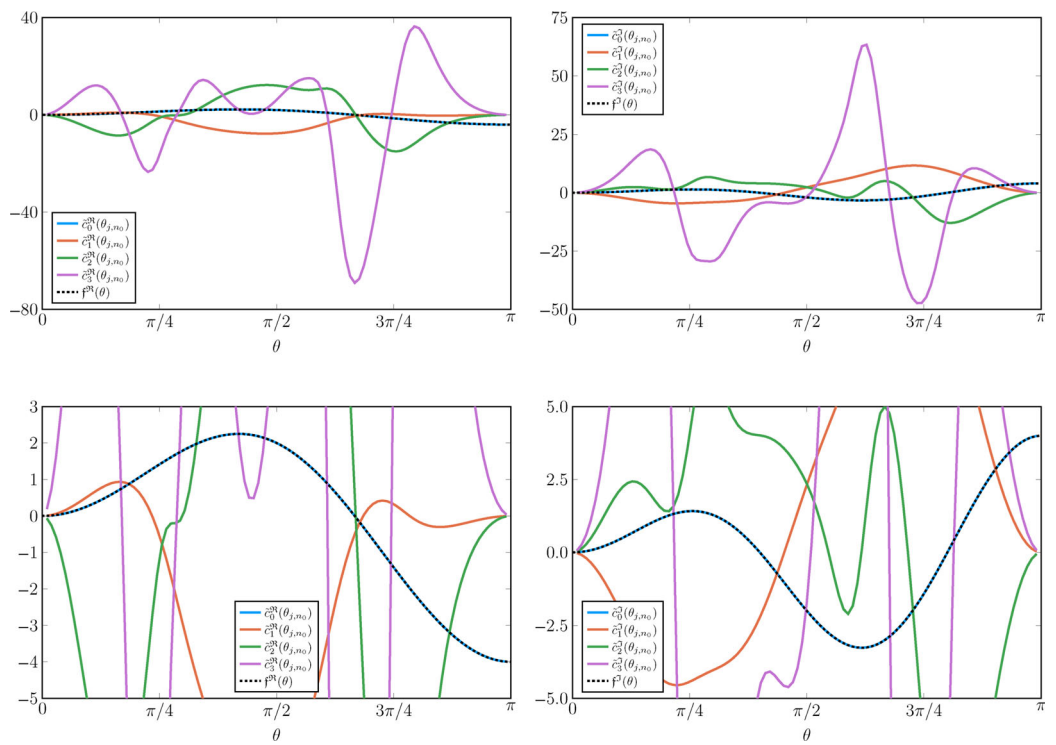


FIGURE 14 [Example 7: generating function $f(\theta) = 2 \cos(\theta) - 2 \cos(2\theta) + i(2 \cos(2\theta) - 2 \cos(3\theta))$] Top Left: The computed $\tilde{c}_k^R(\theta_{j,n_0})$, $k = 0, \dots, \rho$, with $(n_0, \rho) = (100, 4)$ (53 bit) using Algorithm 1. Top Right: The corresponding $\tilde{c}_k^R(\theta_{j,n_0})$ as in the top left panel. Bottom: Detail of the top panels, clearly showing the overlap of $\tilde{c}_0^R(\theta_{j,n_0})$ and $f^R(\theta)$ (bottom left) and $\tilde{c}_0^R(\theta_{j,n_0})$ and $f^R(\theta)$ (bottom right).

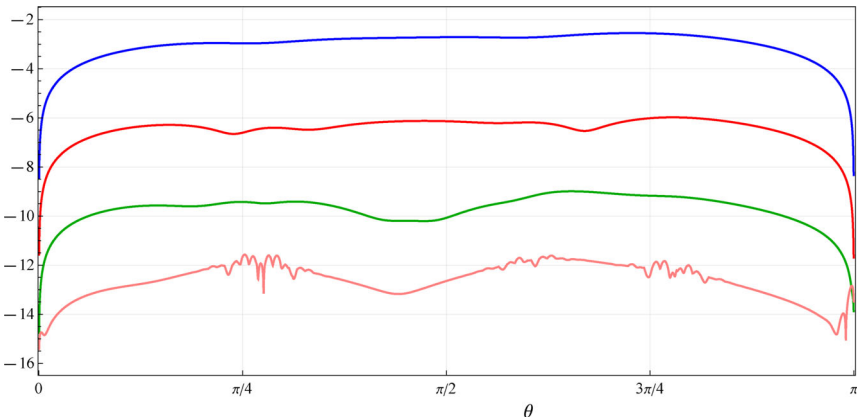


FIGURE 15 [Example 7: generating function $f(\theta) = 2 \cos(\theta) - 2 \cos(2\theta) + i(2 \cos(2\theta) - 2 \cos(3\theta))$] For the Algorithm 1, the base 10 logarithm of the individual eigenvalue errors $E_{j,n}^{NA(\rho)}$ for the Toeplitz matrix $T_n(f)$ with $n = 4096$ and different values of ρ : $\rho = 1$ (blue), $\rho = 2$ (red), $\rho = 3$ (green), and $\rho = 4$ (pink).

approximates the known f^R (bottom left panel) and f^S (bottom right panel) well. Again we recover, to machine precision, the nonzero Fourier coefficients of the symbol f , namely, $\hat{f}_{\pm 1}^R = 1$, $\hat{f}_{\pm 2}^R = -1$, $\hat{f}_{\pm 2}^S = 1$, and $\hat{f}_{\pm 3}^S = -1$.

Figure 15 and Table 3 show the individual and maximum errors $E_{j,n}^{NA(\rho)}(f)$ (see (11)). Figure 15 shows, in particular, how the error decreases, when considering additional terms. As in the previous example, the constant behavior of the normalized errors $(n+1)^\rho E_n^{NA(\rho)}(f)$ in Table 3 proves the applicability of WH (10) until the fourth term. In this case the fifth term generates errors with the same magnitude of the fourth one, hence we can say that WH (10) is applicable only with $\rho \leq 4$ in this case.

TABLE 3 [Example 7: generating function $f(\theta) = 2 \cos(\theta) - 2 \cos(2\theta) + i(2 \cos(2\theta) - 2 \cos(3\theta))$] The maximum eigenvalue errors $E_n^{\text{NA}(\rho)}$ for the Toeplitz matrix $T_n(f)$ with different matrix sizes n and number of terms $\rho = 1, \dots, 4$.

n	256	512	1024	2048	4096
$E_n^{\text{NA}(1)}$	4.4620×10^{-2}	2.2326×10^{-2}	1.1166×10^{-2}	5.5839×10^{-3}	2.7921×10^{-3}
$(n+1)E_n^{\text{NA}(1)}$	1.1467×10^1	1.1453×10^1	1.4450×10^1	1.1441×10^1	1.1439×10^1
$E_n^{\text{NA}(2)}$	2.6822×10^{-4}	6.7308×10^{-5}	1.6857×10^{-5}	4.2224×10^{-6}	1.0562×10^{-6}
$(n+1)^2 E_n^{\text{NA}(2)}$	1.7715×10^1	1.7713×10^1	1.7710×10^1	1.7727×10^1	1.7728×10^1
$E_n^{\text{NA}(3)}$	2.7634×10^{-6}	3.4613×10^{-7}	4.3311×10^{-8}	5.4165×10^{-9}	6.7717×10^{-10}
$(n+1)^3 E_n^{\text{NA}(3)}$	4.6907×10^1	4.6729×10^1	4.6641×10^1	4.6596×10^1	4.6569×10^1
$E_n^{\text{NA}(4)}$	4.9670×10^{-8}	3.1040×10^{-9}	1.9371×10^{-10}	1.9371×10^{-11}	8.1840×10^{-13}
$(n+1)^4 E_n^{\text{NA}(4)}$	2.1668×10^2	2.1498×10^2	2.1382×10^2	2.1105×10^2	2.3058×10^2

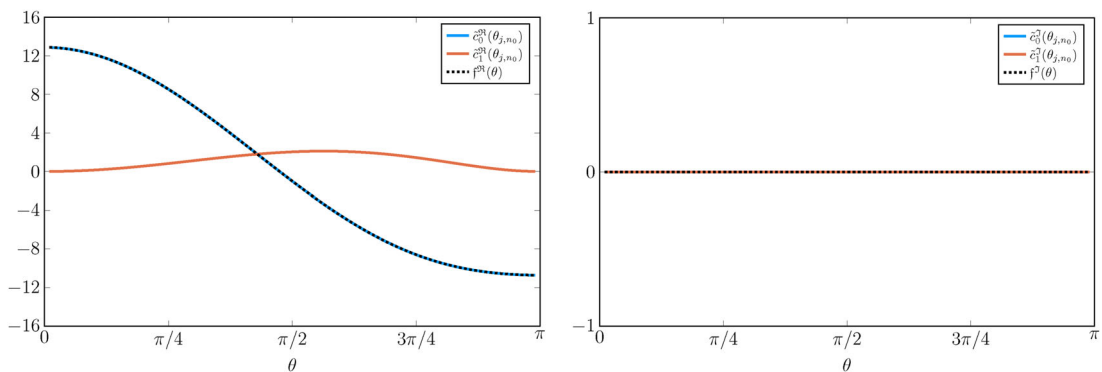


FIGURE 16 [Example 8: generating function $f(\theta) = e^{2i\theta} + ce^{i\theta} + ce^{-i\theta}$ with $c = 6$] Left: The computed $\tilde{c}_k^R(\theta_{j,n_0})$, $k = 0, 1$, with $n_0 = 100$ (1024 bit) using Algorithm 1. Right: The corresponding $\tilde{c}_k^I(\theta_{j,n_0})$ as in the left panel.

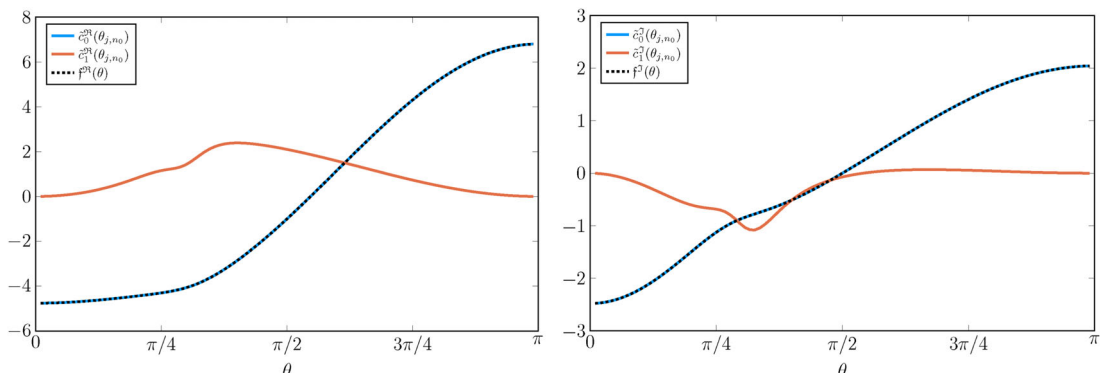


FIGURE 17 [Example 8: generating function $f(\theta) = e^{2i\theta} + ce^{i\theta} + ce^{-i\theta}$] The same as Figure 16 with $c = 3 + i$.

Example 8. In this example we continue the investigation of the generating function in (18) from Example 4. When $c = 6$, the eigenvalues are real and we ordered them from left to right. BigFloat with 1024 bit precision is necessary for this example. In Figures 16 and 17 we show the approximated expansion functions \tilde{c}_k^R (left panels) and \tilde{c}_k^I (right panels) for $(n_0, \rho) = (100, 2)$. Algorithm 1 approximates the unknown f^R (left panel) and f^I (right panel) well.

Figures 18, 19, 20, and Tables 4 and 5 show the individual and maximum errors $E_{j,n}^{\text{NA}(\rho)}(f)$ (see (11)). As in previous examples, the error decreases when considering additional terms but, this time, only through the second one, that is, WH (10) is applicable only with $\rho \leq 2$.

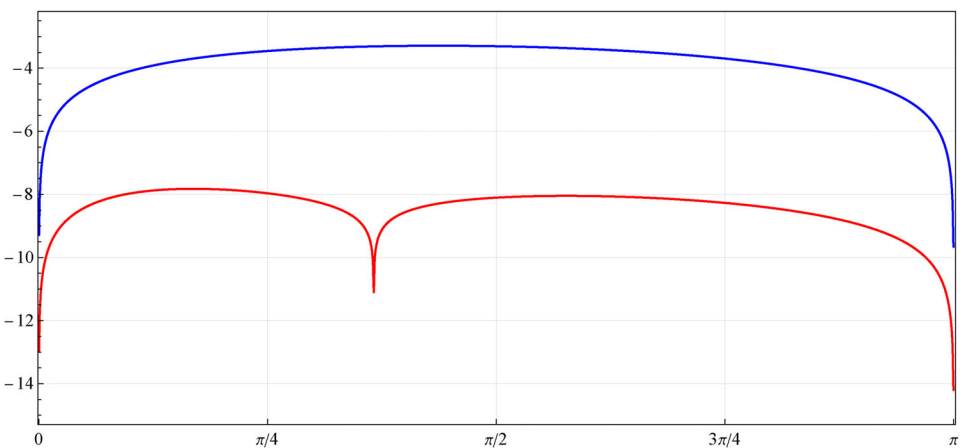


FIGURE 18 [Example 8: generating function $f(\theta) = e^{2i\theta} + ce^{i\theta} + ce^{-i\theta}$ with $c = 6$] For the Algorithm 1, the base 10 logarithm of the individual eigenvalue errors $E_{j,n}^{NA(\rho)}$ for the Toeplitz matrix $T_n(f)$ with $n = 4096$ and ρ terms, $\rho = 1$ (blue) and $\rho = 2$ (red).

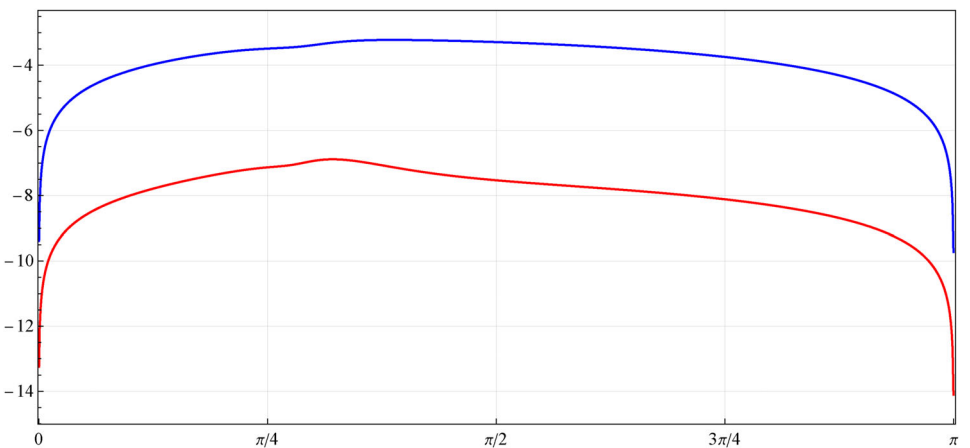


FIGURE 19 [Example 8: generating function $f(\theta) = e^{2i\theta} + ce^{i\theta} + ce^{-i\theta}$] The same as Figure 18 with $c = 3 + i$.

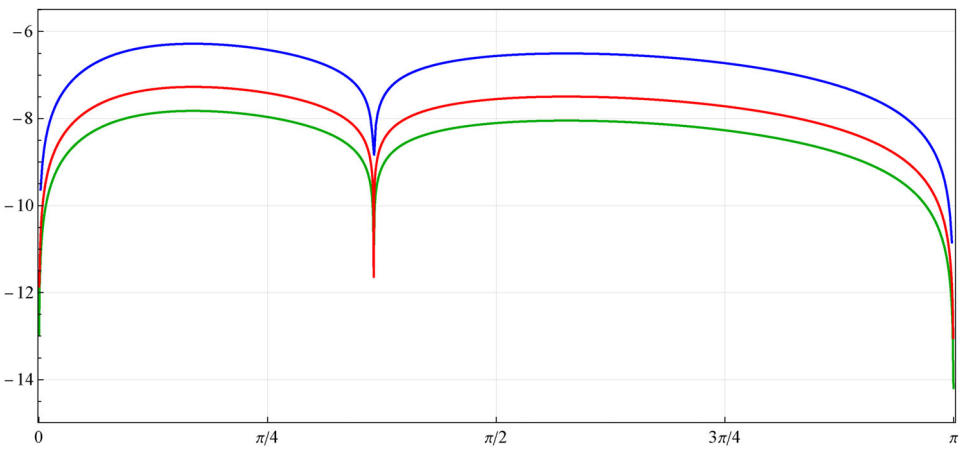


FIGURE 20 [Example 8: generating function $f(\theta) = e^{2i\theta} + ce^{i\theta} + ce^{-i\theta}$ with $c = 6$] For the Algorithm 1, the base 10 logarithm of the individual eigenvalue errors $E_{j,n}^{NA(\rho)}$ for the Toeplitz matrix $T_n(f)$ with $\rho = 2$ and different values of n : $n = 4096$ (green), $n = 2048$ (red), and $n = 1024$ (blue).

TABLE 4 [Example 8: generating function $f(\theta) = e^{2i\theta} + ce^{i\theta} + ce^{-i\theta}$ with $c = 6$] The maximum eigenvalue errors $E_n^{\text{NA}(\rho)}$ for the Toeplitz matrix $T_n(f)$ with different matrix sizes n and number of terms $\rho = 1, 2$.

<i>n</i>	256	512	1024	2048	4096
$E_n^{\text{NA}(1)}$	5.5613×10^{-3}	2.7917×10^{-3}	1.3986×10^{-3}	7.000×10^{-4}	3.5021×10^{-4}
$(n+1)E_n^{\text{NA}(1)}$	1.4292×10^0	1.4321×10^0	1.4336×10^0	1.4344×10^0	1.4348×10^0
$E_n^{\text{NA}(2)}$	3.4011×10^{-6}	5.2384×10^{-7}	1.4678×10^{-8}	5.3469×10^{-8}	1.5017×10^{-8}
$(n+1)^2 E_n^{\text{NA}(2)}$	2.2464×10^{-1}	1.3786×10^{-1}	1.5421×10^{-2}	2.2448×10^{-1}	2.5207×10^{-1}

TABLE 5 [Example 8: generating function $f(\theta) = e^{2i\theta} + ce^{i\theta} + ce^{-i\theta}$] The same as Table 4 with $c = 3 + i$.

<i>n</i>	256	512	1024	2048	4096
$E_n^{\text{NA}(1)}$	5.1625×10^{-3}	2.5873×10^{-3}	1.2952×10^{-3}	6.4807×10^{-4}	3.2421×10^{-4}
$(n+1)E_n^{\text{NA}(1)}$	1.3268×10^0	1.3273×10^0	1.3276×10^0	1.3279×10^0	1.3283×10^0
$E_n^{\text{NA}(2)}$	1.6838×10^{-5}	2.5654×10^{-6}	7.1433×10^{-8}	2.6117×10^{-7}	7.3432×10^{-8}
$(n+1)^2 E_n^{\text{NA}(2)}$	1.1121×10^0	6.7514×10^{-1}	7.5050×10^{-2}	1.0965×10^0	1.2326×10^0

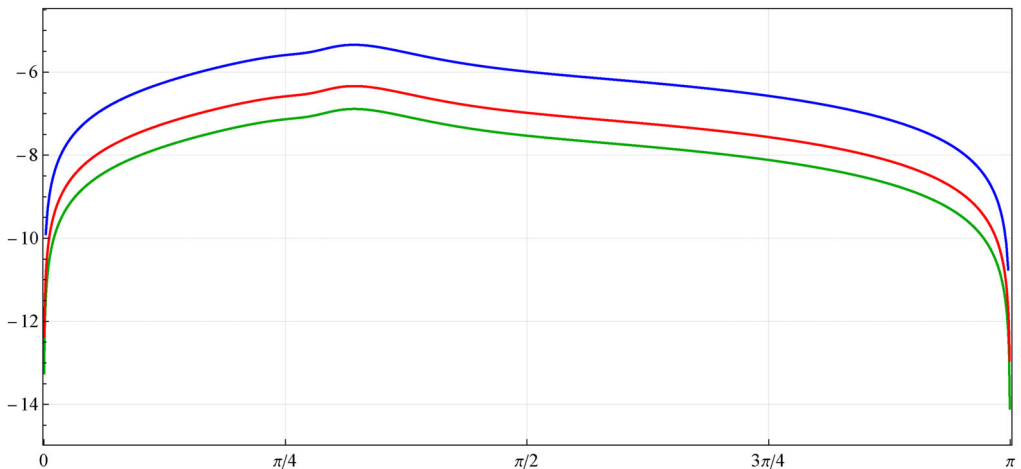


FIGURE 21 [Example 8: generating function $f(\theta) = e^{2i\theta} + ce^{i\theta} + ce^{-i\theta}$] The same as Figure 20 with $c = 3 + i$.

6 | CONCLUSIONS

The Working Hypothesis in the current article concerns the existence of an asymptotic expansion, involving a function \mathfrak{f} describing the eigenvalue distribution of the Toeplitz matrices $T_n(f)$. The assumption is that \mathfrak{f} is complex-valued, as opposed to ¹⁶ where \mathfrak{f} was assumed to be real-valued, and that the generating function f satisfies one of the conditions below

- (i) f belongs to the Tilli class and $\mathcal{ER}(f)$ is connected,
- (ii) the limiting set $\Lambda(f)$ defined in (2) shows one nonclosed analytic arc only.

We have shown in a number of numerical examples that we can recover an accurate approximation of the function \mathfrak{f} . This is done by the matrix-less method described in Algorithm 1, where no information of f or \mathfrak{f} is required, as long as the eigenvalues can be ordered in a consistent way, as n varies. In future investigations, the input argument `eig_fun` could for example encompass preconditioned matrices, matrices generated by matrix-valued symbols, and non-Toeplitz matrices, extracted, for example, from Generalized Locally Toeplitz matrix sequences, stemming from the approximation of variable coefficient differential operators.

The necessity of high-precision data types for the numerical approximation of the eigenvalues is highlighted in the examples, with respectively “constant,” “increasing,” and “quickly increasing” precision requirements.

Splitting the interpolation-extrapolation procedure in Reference 22, into the real and imaginary parts of the spectrum, we used the approximations of c_k^R and c_k^I to efficiently and accurately obtain the eigenvalues of $T_n(f)$. The respective error data is shown in Figures 13, 15, 18–21, and Tables 2–5.

We also approximate the Fourier coefficients \hat{f}_k^R and \hat{f}_k^I , reconstructing f by its Fourier series. In some cases the latter computation could be done to machine precision. The presented algorithm can be a valuable tool for the exploration of the spectral behavior of Toeplitz, Toeplitz-like, and other less understood structured matrices.

For future research, we propose the study of matrices beyond the Toeplitz world, and to use the current results to compute asymptotic expansions for nonmonotone real-valued symbols, and finding new explicit expressions for eigenvalue symbols f .

ACKNOWLEDGMENTS

The authors want to acknowledge Carlo Garoni for valuable discussions and suggestions. Part of the numerical experiments were calculated in the computer center Jürgen Tischer of the mathematics department at Universidad del Valle. Furthermore, the work of Stefano Serra-Capizzano was funded from the European High-Performance Computing Joint Undertaking (JU) under grant agreement number 955701. The JU receives support from the European Union’s Horizon 2020 research and innovation programme and Belgium, France, Germany, and Switzerland. Finally Stefano Serra-Capizzano is grateful for the support of the Italian Agency GNCS and of the Laboratory of Theory, Economics and Systems—Department of Computer Science at Athens University of Economics and Business.

DATA AVAILABILITY STATEMENT

Data sharing not applicable to this article as no datasets were generated or analyzed during the current study.

ORCID

Manuel Bogoya  <https://orcid.org/0000-0003-3551-8152>

Sven-Erik Ekström  <https://orcid.org/0000-0002-7875-7543>

Stefano Serra-Capizzano  <https://orcid.org/0000-0001-9477-109X>

Paris Vassalos  <https://orcid.org/0000-0002-2131-7643>

REFERENCES

1. Böttcher A, Silbermann B. Introduction to large truncated Toeplitz matrices. Universitext. New York: Springer-Verlag; 1999.
2. Böttcher A, Grudsky SM. Spectral properties of banded Toeplitz matrices. Philadelphia: Society for Industrial and Applied Mathematics (SIAM); 2005.
3. Garoni C, Serra-Capizzano S. Generalized locally Toeplitz sequences: theory and applications. Vol I. Cham: Springer; 2017.
4. Garoni C, Serra-Capizzano S. Generalized locally Toeplitz sequences: theory and applications. Vol II. Cham: Springer; 2018.
5. Garoni C, Speleers H, Ekström SE, Reali A, Serra-Capizzano S, Hughes T. Symbol-based analysis of finite element and isogeometric B-spline discretizations of eigenvalue problems: exposition and review. Arch Comput Method E. 2019;26(5):1639–90.
6. Grenander U, Szegő G. Toeplitz forms and their applications. California monographs in mathematical sciences. 2nd ed. New York: Chelsea Publishing Co; 1984.
7. Widom H. Eigenvalue distribution of nonselfadjoint Toeplitz matrices and the asymptotics of Toeplitz determinants in the case of nonvanishing index. Topics in operator theory: Ernst D. Hellinger memorial volume. Operator Theory: Advances and Applications. Volume 48. Basel: Birkhäuser; 1990. p. 387–421.
8. Tili P. Some results on complex Toeplitz eigenvalues. J Math Anal Appl. 1999;239(2):390–401.
9. Tili P. A note on the spectral distribution of Toeplitz matrices. Linear Multilin Algebra. 1998;45(2-3):147–59.
10. Serra-Capizzano S. On the extreme eigenvalues of Hermitian (block) Toeplitz matrices. Linear Algebra Appl. 1998;270:109–29.
11. Böttcher A, Grudsky SM. On the condition numbers of large semi-definite Toeplitz matrices. Linear Algebra Appl. 1998;279(1/3):285–301.
12. Schmidt P, Spitzer F. The Toeplitz matrices of an arbitrary Laurent polynomial. Math Scand. 1960;8:15–38.
13. Hirschman Jr, II. The spectra of certain Toeplitz matrices. Illinois J Math. 1967;11:145–59.
14. Day KM. Measures associated with Toeplitz matrices generated by the Laurent expansion of rational functions. Trans Amer Math Soc. 1975;209:175–83.
15. Böttcher A, Gasca J, Grudsky SM, Kozak AV. Eigenvalue clusters of large tetradagonal Toeplitz matrices. Integr Equat Oper Th. 2021;93(1):1–27.
16. Ekström SE, Vassalos P. A matrix-less method to approximate the spectrum and the spectral function of Toeplitz matrices with real eigenvalues. Numer Algorithms. 2022;89:701–20.

17. Bogoya M, Böttcher A, Grudsky SM, Maximenko EA. Eigenvalues of Hermitian Toeplitz matrices with smooth simple-loop symbols. *J Math Anal Appl.* 2015;422:1308–34.
18. Batalshchikov AA, Grudsky SM, Malisheva IS, Mihalkovich SS, Ramirez de Arellano E, Stukopin VA. Asymptotics of eigenvalues of large symmetric Toeplitz matrices with smooth simple-loop symbols. *Linear Algebra Appl.* 2019;580:292–335.
19. Ekström SE, Garoni C, Serra-Capizzano S. Are the eigenvalues of banded symmetric Toeplitz matrices known in almost closed form? *Exper Math.* 2018;27(4):478–87.
20. Ahmad F, Al-Aidarous ES, Alrehaili DA, Ekström SE, Furci I, Serra-Capizzano S. Are the eigenvalues of preconditioned banded symmetric Toeplitz matrices known in almost closed form? *Numer Algorithms.* 2018;78(3):867–93.
21. Ekström SE, Furci I, Serra-Capizzano S. Exact formulae and matrix-less eigensolvers for block banded Toeplitz-like matrices. *BIT Num Math.* 2018;58(4):937–68.
22. Ekström SE, Garoni C. A matrix-less and parallel interpolation-extrapolation algorithm for computing the eigenvalues of preconditioned banded symmetric Toeplitz matrices. *Numer Algorithms.* 2019;80:819–48.
23. Ekström SE, Furci I, Garoni C, Manni C, Serra-Capizzano S, Speleers H. Are the eigenvalues of the B-spline isogeometric analysis approximation of $-\Delta u = \lambda u$ known in almost closed form? *Numer Linear Algebra Appl.* 2018;25(5):e2198, 34 pp.
24. Beam R, Warming R. The asymptotic spectra of banded Toeplitz and quasi-Toeplitz matrices. *SIAM J Sci Comput.* 1993;14(4):971–1006.
25. Fisher ME, Hartwig RE. Toeplitz determinants some applications, theorems, and conjectures. *Adv Chem Phys.* 1968;15:333–53.
26. Böttcher A, Silbermann B. Analysis of Toeplitz operators. Springer monographs in mathematics. 2nd ed. Berlin: Springer-Verlag; 2006.
27. Bogoya M, Böttcher A, Grudsky SM. Asymptotics of individual eigenvalues of a class of large Hessenberg Toeplitz matrices. *Oper Theory Adv Appl.* 2012;220:77–95.
28. Bogoya M, Grudsky SM, Maximenko EA. Eigenvalues of Hermitian Toeplitz matrices generated by simple-loop symbols with relaxed smoothness. *Oper Theory Adv Appl.* 2017;259:179–212.
29. Bogoya M, Böttcher A, Grudsky SM, Maximenko EA. Eigenvalues of Hessenberg Toeplitz matrices generated by symbols with several singularities. *Commun Math Anal.* 2011;3:23–41.
30. Bogoya M, Grudsky SM, Mazza M, Serra-Capizzano S. On the extreme eigenvalues and asymptotic conditioning of a class of Toeplitz matrix-sequences arising from fractional problems. *Linear Multilin Algebra.* 2022;71(15):2462–73.
31. Bogoya M, Grudsky SM, Serra-Capizzano S, Tablino-Possio C. Fine spectral estimates with applications to the optimally fast solution of large FDE linear systems. *BIT Numer Math.* 2022;62:1417–31.
32. Donatelli M, Mazza M, Serra-Capizzano S. Spectral analysis and structure preserving preconditioners for fractional diffusion equations. *J Comput Phys.* 2016;307:262–79.
33. Olver F. Asymptotics and special functions. In: Peters AK, ed. AKP classics. Wellesley, MA: A K Peters, Ltd.; 1997.
34. Böttcher A, Grudsky SM, Maximenko EA. Inside the eigenvalues of certain Hermitian Toeplitz band matrices. *J Comput Appl Math.* 2010;233(9):2245–64.
35. Barrera M, Böttcher A, Grudsky SM, Maximenko EA. Eigenvalues of even very nice Toeplitz matrices can be unexpectedly erratic. *Oper Theory: Adv Appl.* 2018;268:51–77.
36. Bogoya M, Serra-Capizzano S. Eigenvalue superposition expansion for Toeplitz matrix-sequences, generated by linear combinations of matrix-order dependent symbols, and applications to fast eigenvalue computations. arXiv:211211794 2022.
37. Ekström SE. Approximating the perfect sampling grids for computing the eigenvalues of Toeplitz-like matrices using the spectral symbol. arXiv:190106917 2019.
38. Bogoya M, Ekström SE, Serra-Capizzano S. Fast Toeplitz eigenvalue computations joining interpolation-extrapolation matrix-less algorithms and simple-loop theory. *Numer Algorithms.* 2022;91:1653–76.
39. Bezanson J, Edelman A, Karpinski S, Shah V. Julia: a fresh approach to numerical computing. *SIAM Rev.* 2017;59(1):65–98.
40. Trefethen LN, Embree M. Spectra and pseudospectra: the behavior of nonnormal matrices and operators. Princeton, New Jersey: Princeton University Press; 2005.
41. Reichel L, Trefethen LN. Eigenvalues and pseudo-eigenvalues of Toeplitz matrices. *Linear Algebra Appl.* 1992;162–164:153–85.
42. Ekström SE. Matrix-less methods for computing eigenvalues of large structured matrices. Uppsala University, PhD Thesis, Uppsala: Acta Universitatis Upsaliensis 2018. Available from: <http://urn.kb.se/resolve?urn=urn:nbn:se:uu:diva-346735>

How to cite this article: Bogoya M, Ekström S-E, Serra-Capizzano S, Vassalos P. Matrix-less methods for the spectral approximation of large non-Hermitian Toeplitz matrices: A concise theoretical analysis and a numerical study. *Numer Linear Algebra Appl.* 2024;e2545. <https://doi.org/10.1002/nla.2545>